A FINE-RESOLUTION BAROTROPIC MODEL OF THE NORTH ATLANTIC DRIVEN BY WIND AND ATMOSPHERIC PRESSURE FORCING

YOUYU LU

A FINE-RESOLUTION BAROTROPIC MODEL OF THE NORTH ATLANTIC DRIVEN BY WIND AND ATMOSPHERIC PRESSURE FORCING

By

©Youyu Lu, B.Eng., M.Sc.

A thesis submitted to the School of Graduate

Studies in partial fulfillment of the

requirements for the degree of

Master of Science

Department of Physics

Memorial University of Newfoundland

March, 1994

St. John's Newfoundland Canada

ISBN 0-315-91645-1

Canada

Abstract

We investigate the response of the North Atlantic to wind and atmospheric pressure forcing with a two-dimensional, fine-resolution barotropic model. The model domain extends from the equator to 65°N and from 100 °W to 14°E with a resolution of 1/3° in latitude and 2/5° in longitude. The forcing field to drive the model is the twice-daily wind and atmospheric pressure data from the European Center for Medium Range Weather Forecasts (ECMWF). The model results are compared with sea level observed at coastal tide gauges, volume transport derived from voltage measurements made using a submarine cable across the Florida Straits, and bottom pressure data collected on the Labrador and Newfoundland Shelf. The time scales being studied range from several days to seasonal.

The primary model experiment is a two-year (1985-1986) run driven by both wind and atmospheric pressure forcing. Three one-year runs are used to determine the contributions from the individual forcing, and the influence of Hudson Bay on the Labrador Shelf. Model results show the best agreement with observed sea level data at locations with broad shelves where the stratification is weak. Significant coherence between observed and modeled adjusted sea level is obtained at periods beyond ~3 days, at four representative stations along the western boundary. Contributions from

atmospheric pressure forcing are not important for periods beyond ~2-3 days. The primary model experiment explains the observed volume transport variation through the Florida Straits at synoptic time scales, which is mainly due to wind. The model captures the variation at longer time scales in 1985, but not in 1986. The exclusion of advection by the mean flow may be the reason for the drop of coherence at ~10 days in the case of the Florida Straits volume transport and at ~12 days in the case of sea level at Fernandina Beach, Florida.

Model output is also coherent with the observed bottom pressure data from the Labrador and Newfoundland Shelf. The significant non-isostatic response in the observational data at synoptic time scales is reproduced by model experiments with the Hudson Bay-Hudson Strait system included, with energy peaks at ~2-6 days. The contribution from atmospheric pressure forcing is only important in generating the energy peak at ~2-6 days when the Bay/Strait system is included, verifying the Helmholtz-like resonance mechanism proposed by former researchers. Wind forcing dominates over atmospheric pressure forcing at synoptic time scales. In particular, the wind over Hudson Bay–Hudson Strait is shown to be important.

Acknowledgments

My study in the Physical Oceanography Group at Memorial University of Newfoundland has been supervised by Drs. Richard J. Greatbatch and Brad de Young. I greatly appreciate their choice of thesis topic and the guidance they offered during the work. I benefited a lot from their profound understanding of ocean dynamics and plentiful experiences in research work. Their comments on the manuscript and patience reviewing greatly improved this thesis.

This work is part of an ongoing effort of the Group. The nicely written programmes by Allan Goulding and H. Todd Wareham greatly facilitated my study. Assistance in dealing with computer related problems was also provided by Ying Ren and Ken Forward. Without their help, I could not have finished this work in such a short time.

My education at MUN also benefited from Drs. Alex Hay and Kevin Lamb through the courses they taught. I would also like to take the opportunity to thank Prof. Shizuo Feng at Ocean University of Qingdao, who brought me to the field of physical oceanography and offered encouragement to me from my home country, China.

I am grateful to many people here, in particular Guoqing Li and Fraser David-

son, for the friendship they offered during my study in Newfoundland. My wife and both our parents offered tremendous help enabling me to accept the opportunity to study abroad. I owe a great debt to them.

This work has been funded by the Natural Sciences and Engineering Research Council of Canada (NSERC) through grants awarded to Drs. Greatbatch and de Young. Financial support from the School of Graduate Studies at MUN, in the form of a Graduate Fellowship, is also acknowledged.

Contents

List of Figures

List of Tables

Chapter 1

Introduction

The motivation of the present study is to determine how well a simple barotropic model, driven by realistic wind and atmospheric pressure forcing, can explain variability in observed sea level, volume transport and bottom pressure data from the North Atlantic. The time scales examined span from several days to seasonal, the periods at which the barotropic response is expected to dominate.

Atmospheric forcing (wind and pressure) is one of the major excitations and energy inputs to the ocean. Other forcing may come from the variation in the relative position of the earth with the moon and sun, causing tides; or the uneven heating and fresh water input at the ocean surface, which drives the thermohaline circulation. In reality, the atmospheric forcing consists of a broad-band spectrum, both in time and

space. The nature of the oceanic response to external forcing depends largely on the spatial and time scales.

The effect of atmospheric pressure forcing is evident in inducing sea level variations. A major part of the sea level response can be modeled using the inverted barometer (IB) approximation (Gill and Niiler, 1973). The IB approximation implies an equilibrium oceanic response in which sea level gradients perfectly offset the horizontal gradients in atmospheric pressure fields. The IB response is dynamically unimportant as there are no currents associated with it. It is the deviation from IB, or the non-isostatic response associated with atmospheric pressure forcing, that is of dynamical interest. The recent work of Ponte et al. (1991), Ponte (1993) and de Young et al. (1994) addressed the breakdown of the IB approximation using coarse resolution numerical models. A general conclusion can be drawn from these studies is that the IB approximation is generally valid at periods beyond 2 days, but failure at longer periods occurs over extensive regions. The non-isostatic sea level variation tends to amplify near boundaries. However, these models are too coarse to examine the response at the coast and in shelf regions, where more observational data are available. Garrett et al. (1985) found a significant non-isostatic response at synoptic time scales (~2-10 days), in the sea level data at Nain, Labrador. Wright et al. (1987) attributed this unusual response to the influence from a resonant response

of the Hudson Bay- Hudson Strait system to atmospheric pressure forcing. Clearly models capable of resolving the shelf areas and adjacent shallow seas are called for to clarify this point.

Studies of the oceanic response to wind stress forcing have been summarized in section 12.4 of Gill (1982). Using a numerical model under idealized wind forcing, Anderson et al. (1979) studied the transient response of the ocean at short (up to 100 days) and long (up to *years*) time scales. They showed that at short time scales, a rapid barotropic adjustment takes places within a few days, giving rise to a topographically modified Sverdrup flow in the ocean interior. This response is essentially the same as in an unstratified ocean. In the meanwhile, baroclinic adjustment modifies the barotropic response and at long time scales a final state with all the motion being confined near the surface is established. At midlatitudes, the baroclinic adjustment is so slow that barotropic dynamics is expected to be important at seasonal time scales. Gill and Niiler (1973) obtained the same result based on a scaling argument. Greatbatch and Goulding (1989, hereinafter referred to as GG) presented their results on the seasonal variations in the North Atlantic, with a $1^o \times 1^o$ resolution barotropic model run using the monthly mean seasonally varying surface wind stress forcing of Hellerman and Rosenstein (1983). Their model successfully reproduced the phase of the seasonal cycle in adjusted sea level, corrected for the steric effect,

at stations along the southeastern seaboard of the United States and at St. John's, Newfoundland. The model also reproduced the seasonal cycle of volume transport through the Florida Straits, although it underestimated the amplitude.

Wind forcing plays a role partly by causing local wind set-up and partly by changing the large scale ocean circulation. Processes related to wind forcing in coastal waters vary from storm surges, coastal trapped waves, to coastal circulation (Csanady, 1982). Greatbatch et al. (1990) applied the same model as GG's to the Labrador and Newfoundland Shelf. Their model had a finer resolution ($1/4^{\circ} \times 1/4^{\circ}$) to resolve the Shelf, and introduced the influence of the rest of the North Atlantic by combining the output of GG's coarse resolution North Atlantic at the open boundary. Seasonal variation in sea level was studied. A similar study, by de Young et al. (1992), addressed the variation at synoptic time scales. Contributions from both local set-up and large scale influence were found to be important on the Shelf.

As is well known, there are several large numerical ocean circulation models presently being run by a number of research groups in the world. The most distinguished models are the Bryan-Cox-Semtner model (see e.g., Bryan, 1969; Cox, 1984) and its successors, e.g., the free-surface version of Killworth et al. (1991) and the eddy-resolving WOCE-CME (the World Ocean Circulation Experiment, Community Modelling Effort, see Bryan and Holland, 1989). These models, intended to investi-

gate the overall motions in the world oceans, form the mainstream of the numerical ocean circulation studies. As these large models are physically complex and computationally costly, simple models can provide some help, in certain aspects, to understand the behavior of the more complex models. For example, Fanning et al. (1994) studied the seasonal transport variations through the Florida Straits using a barotropic model forced with different wind stress climatologies. They made a comparison of their simple model results with those of Böning et al. (1991), who used the Kiel version of the WOCE-CME. Both agreement and disagreement between the two models were found, providing insight into the dynamical processes at work.

The model used in the present work is similar to that used by GG. The rigid-lid approximation as used in their model is now relaxed and the integration is performed in the time domain (GG did their calculations in frequency space by replacing $\partial/\partial t$ with $i\omega$, this method being feasible only for a linear system). The rigid-lid approximation eliminates surface gravity waves and enables large time steps to be taken, and is adopted by most versions of the Bryan-Cox-Semtner model except that of Killworth et al. (1991). Two of the reasons Killworth et al. argued in favor of free-surface models are (i) it enables the direct assimilation of altimetric data into ocean models, which will play an important role in the generation of ocean prediction models, and (ii) it allows tides to be included, which are believed to play a role in affecting mixing

processes. The study of the non-isostatic response to atmospheric pressure forcing also needs a free-surface model. We also expect surface gravity waves to play some role in the high frequency response, since the basinwide resonance for the North Atlantic has a period of about a day (Ponte et al., 1991). Moreover, although not done here, nonlinear interactions of tidal currents and their interactions with atmospheric driven currents, the effects of which cannot easily be removed by harmonic analysis, can only be included with a free-surface model.

The use of forcing fields, more representative of reality, was called for by Willebrand et al. (1980). The forcing fields adopted to drive the model in the present work consist of the wind and atmospheric pressure dataset from the European Center for Medium Range Weather Forecasts (ECMWF). These data are a combination of observations and model nowcast results and are the best available data to use in regions where observations are sparse. ECMWF forcing was used by Ponte (1993) and de Young et al. (1994) to study the non-isostatic response of sea level in their global models. The ECMWF wind forcing was used also by de Young et al. (1992) in their study of the bottom pressure variability on the Labrador shelf. The ECMWF data are twice-daily and long time series are available. This enables our study on the model behavior to cover a wide period range, from several days to many months.

Our model results will be compared with three observational datasets. They

are, respectively, sea level from an array of tide gauges along the coast around the North Atlantic; the daily mean volume transports through the Florida Straits, as derived from voltage measurements using a submarine cable (Larsen, 1992); and bottom pressure data collected on the Labrador and Newfoundland Shelf between summer 1985 and summer 1987 (Wright et al., 1988).

The plan of this thesis is as follows. In the next chapter, an introduction to the model and the design of the model experiments is given. Comparisons of the model results with observational data are given in chapters 3-5. The results for sea level variations at stations along the coast of the North Atlantic are presented first (chapter 3), followed by an investigation on the volume transport variation through the Florida Straits (chapter 4). An intensive study on the bottom pressure variability on the Labrador and Newfoundland Shelf is reported in chapter 5. Summary and conclusions are provided in chapter 6.

Chapter 2

The Model

2.1 The Governing Equations

We work with the vertically integrated, linearized shallow water equations for a homogeneous ocean, forced by wind and atmospheric pressure variation (e.g., Gill, 1982). In spherical coordinates, these are

$$\frac{\partial \eta}{\partial t} + \frac{1}{a\cos\phi}\left[\frac{\partial}{\partial \lambda}(Hu) + \frac{\partial}{\partial \phi}(Hv\cos\phi)\right] = 0 \tag{2.1}$$

$$\frac{\partial u}{\partial t} - 2\Omega \sin\phi\, v = -\frac{g}{a\cos\phi}\frac{\partial}{\partial \lambda}\left(\eta + \frac{p_a}{\rho_o g}\right) + \frac{(\tau_s^\lambda - \tau_b^\lambda)}{\rho_o H} + A_h f^\lambda \tag{2.2}$$

$$\frac{\partial v}{\partial t} + 2\Omega \sin\phi\, u = -\frac{g}{a}\frac{\partial}{\partial \phi}\left(\eta + \frac{p_a}{\rho_o g}\right) + \frac{(\tau_s^\phi - \tau_b^\phi)}{\rho_o H} + A_h f^\phi \tag{2.3}$$

where λ is longitude, ϕ is latitude, u and v are the eastward and northward components of velocity, η is the upwards displacement of sea level, p_a is atmospheric pressure, Ω the rotation rate of the earth, a the radius of the earth, g the acceleration due to gravity, ρ_o is a representative density for sea water (taken here to be 1025 kg m^{-3}), H is the depth of the ocean. τ_s^λ and τ_s^ϕ are the eastward and northward components of the surface wind stress, which are computed following Large and Pond (1981). τ_b^λ and τ_b^ϕ are the bottom stress components, which can be related to the velocity field either by a linear bottom friction law

$$(\tau_b^\lambda, \tau_b^\phi)/\rho_o = r(u, v) \tag{2.4}$$

or by a quadratic law

$$(\tau_b^\lambda, \tau_b^\phi)/\rho_o = k(u^2 + v^2)^{1/2}(u, v) \tag{2.5}$$

with r and k, the linear and quadratic bottom friction coefficients respectively, both empirical constants. Finally, f^λ and f^ϕ represent the effects of horizontal eddy viscosity and can be parameterized as (see Bryan, 1969)

$$f^\lambda = \frac{1}{a^2\cos^2\phi}\frac{\partial^2 u}{\partial\lambda^2} + \frac{1}{a^2\cos\phi}\frac{\partial}{\partial\phi}(\cos\phi\frac{\partial u}{\partial\phi}) + \frac{1}{a^2}[(1-\tan^2\phi)u - \frac{2\tan\phi}{\cos\phi}\frac{\partial v}{\partial\lambda}] \tag{2.6}$$

$$f^\phi = \frac{1}{a^2\cos^2\phi}\frac{\partial^2 v}{\partial\lambda^2} + \frac{1}{a^2\cos\phi}\frac{\partial}{\partial\phi}(\cos\phi\frac{\partial v}{\partial\phi}) + \frac{1}{a^2}[(1-\tan^2\phi)v + \frac{2\tan\phi}{\cos\phi}\frac{\partial u}{\partial\lambda}] \tag{2.7}$$

To close the problem we need to set the lateral boundary condition. As our model domain covers almost the whole North Atlantic basin (from the equator to

65°N), we close the north and south boundaries just as at the coast. A "no-slip" condition is set along all the boundaries, including boundaries of islands. The equator is a natural boundary as it as acts as a waveguide, i.e., disturbances are trapped in the vicinity of the equator (Gill, 1982).

The above problem is a linear one if the linear law of bottom friction is adopted. (the advection terms have been neglected because the velocities in the solution are small). The nonlinearity introduced by the quadratic law is expected to be unimportant.

2.2 The Method of Solution

Unlike models involving the rigid-lid approximation, our mass-conservation equation (2.1) includes the free-surface variation. This avoids the introduction of a stream-function to replace the velocity components. Thus we must work with the primitive equations.

A finite-difference method, similar to that designed by Heaps (1971), is used to solve the above problem. The centered differencing for the spatial differential operators is performed on the staggered C-grid of Mesinger and Arakawa (1976), with an η grid-point surrounded by two u points at the same latitude and two v points

at the same longitude (see Fig.4 of GG). A forward-in-time differencing scheme is applied to equation (2.1) to calculate η. A backward-in-time scheme is applied to equations (2.2) and (2.3) to calculate u and v, except that the lateral friction terms are treated explicitly. The Coriolis terms are calculated by averaging the updated values of v at four v-grid points surrounding a u-grid point or averaging u at four u-grid points surrounding a v-grid point. The bottom friction terms are treated implicitly for the linear case but of a mixed type for the quadratic case (the part $k(u^2 + v^2)^{1/2}$ is explicit).

The most important stability condition for the finite-difference scheme described above is the Courant-Friedrichs-Lewy (CFL) criterion

$$\Delta t \leq \sqrt{\frac{2}{gh}}(\frac{\Delta s}{2}) \tag{2.8}$$

where Δs is the minimum grid spacing between grid points of the same variables. For our model domain with a resolution of $1/3^o$ in latitude and $2/5^o$ in longitude, (2.8) requires the maximum time step to be no larger than 60 seconds. We use a time step of 60 seconds in our model experiments and the calculations are found to be stable.

2.3 The Inverse Barometer Effect

In equations (2.2) and (2.3), the atmospheric pressure term, $p_a/\rho_o g$, can be replaced by

$$-\eta_a = \frac{1}{\rho_o g}(p_a - \overline{p_a}) \tag{2.9}$$

where $\overline{p_a}$ is a spatial average of p_a, η_a is the surface elevation called the inverse barometer(IB) response. In the atmospheric pressure-only case, $\eta = \eta_a$ implies an equilibrium oceanic response in which sea level gradients perfectly offset the horizontal gradient in atmospheric pressure fields (Gill, 1982). No currents are generated when the IB response is established (refer to equations (2.2)-(2.3)). For this reason, the pressure-induced sea level slopes are not dynamically significant and are usually subtracted from observed sea level data. It is the remaining part, namely the adjusted sea level η' defined by

$$\eta' = \eta - \eta_a \tag{2.10}$$

that is of dynamical interest.

In calculating η_a with equation (2.9), the spatial average of atmospheric pressure, $\overline{p_a}$, should be compated over the global oceans to ensure the total volume of sea water is constant (taking the sea water to be incompressible). The IB response involves contributions from both local and nonlocal atmospheric pressure fluctua-

tions, i.e., η_a can change with $\overline{p_a}$ even when the local p_a remains constant (Ponte et al., 1991). If $\overline{p_a}$ is constant, then the "local" IB approximation results, i.e. changes in sea surface elevation are induced only by changes in local atmospheric pressure (1 mbar increase in p_a corresponds to approximately 1 cm decrease in η_a). In reality, however, $\overline{p_a}$ varies with time (see Fig. 3 in Ponte, 1993), and the nonlocal influence of atmospheric pressure fluctuations must be taken into account. The IB response of sea level calculated with equation (2.9) can be removed from observed sea level (according to equation (2.10)) to compare with model-calculated adjusted sea level.

Since the model in the present study is not global, but has a limited domain (the North Atlantic), the average of p_a over the model domain is used in (2.9) to calculate the IB response of the model. This ensures the total volume of sea water within the model domain is constant. Model-calculated adjusted sea level is then obtained using (2.10) to remove the IB response from model-calculated sea level.

Adjusted sea level can be related to variations in ocean bottom pressure, p_b'. In a uniform density ocean and following the hydrostatic approximation, the relation is derived as

$$p_b' = \rho_o g \eta' + \overline{p_a}' \tag{2.11}$$

with $\overline{p_a}'$ is the time-varying part of $\overline{p_a}$, the atmospheric pressure averaged over global

ocean, and η' is the adjusted sea level. The local IB response has no contribution to bottom pressure variation. The contribution from the nonlocal IB response, $\overline{p_a}'$, is estimated to be small compared with η' (the amplitude of $\overline{p_a}'$ is only $\sim$1.5 mbar from the ECMWF data; see Fig. 3 in Ponte, 1993). In Chapter 5 we compare the model-calculated adjusted sea level directly with observed bottom pressure, i.e., 1 cm increase in adjusted sea level corresponds to roughly 1 mbar increase in p_b'.

2.4 Model Experiments

The bottom topography adopted in our model experiments is the same as that used by Bryan and Holland (1989) in their eddy-resolving general circulation model, except that our model domain extends from 0°N to 65°N and from 100°W to 14°E and the Hudson Bay–Hudson Strait system is included (Fig. 2.1). The resolution is 1/3° in latitude and 2/5° in longitude, giving an equal grid spacing in the north-south and east-west directions of about 37 km at 34°N. This topography is stepwise (with 30 discrete depth levels) and designed for three-dimensional, level models. The topography of the Hudson Bay/Hudson Strait is first extracted from a digital terrain dataset (with a resolution of 1/12° × 1/12°), then linearly interpolated to the 2/5° × 1/3° grid and discretized to the closest discrete level, and finally merged with the North

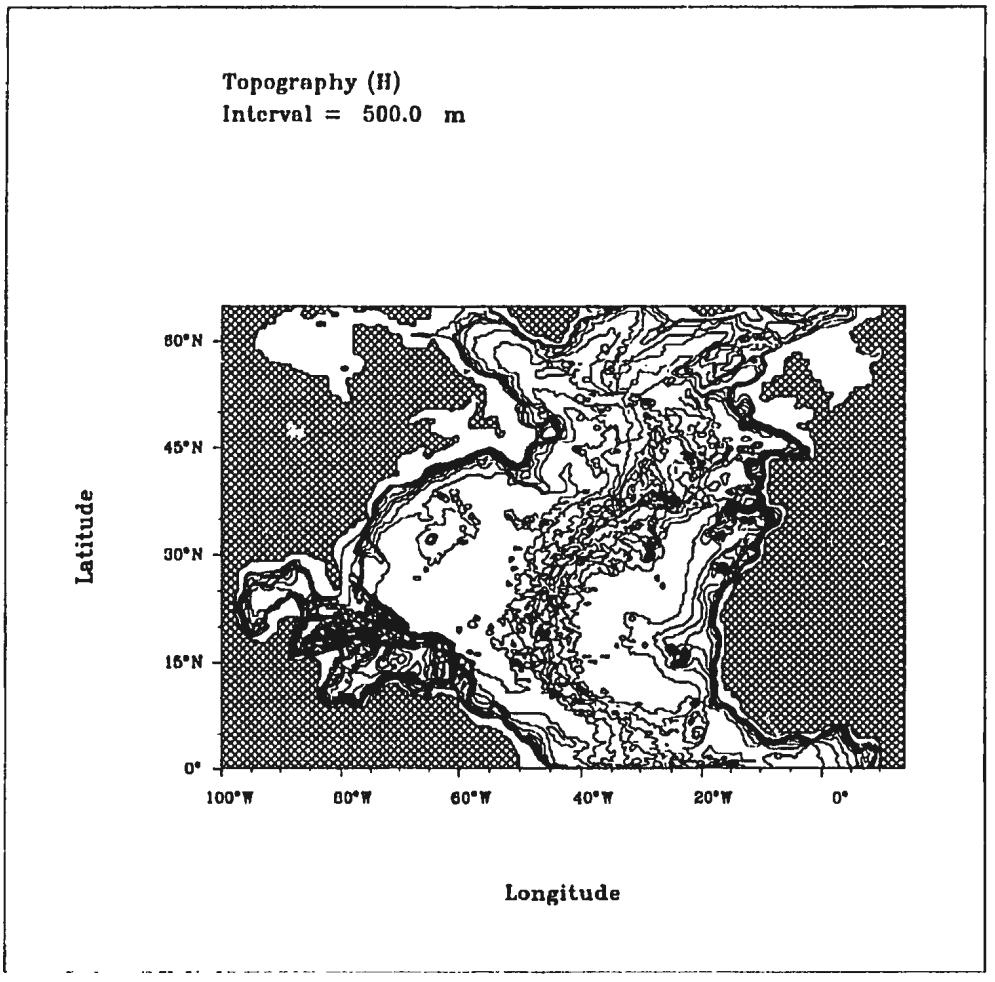

Figure 2.1: Bottom topography of the model domain. The contour interval is 500m.

Table 2.1: List of model experiments

#	Forcing Field	Model Domain
EXP1	wind and pressure	whole domain
EXP2	pressure only	whole domain
EXP3	wind and pressure	Hudson Bay closed
EXP4	pressure only	Hudson Bay closed

Atlantic topography. In some of the model experiments, the Hudson Bay Hudson Strait system is closed in order to determine its influence on the Labrador and Newfoundland Shelf.

The model input is provided by the wind and atmospheric pressure fields from the European Center for Medium Range Weather Forecasts (ECMWF). The ECMWF data is twice-daily (sampled at 0 and 12 hour GMT each day) with a spatial resolution of $2.5^o \times 2.5^o$. These data are interpolated to the same resolution as the topography using the technique of Akima (1978) and then linearly interpolated to each time step.

The model experiments described in the following chapters are listed in Table 2.1. The primary experiment, EXP1, is a two-year (1985-1986) calculation using both wind and atmospheric pressure forcing over the whole domain, i.e., the Hudson Bay–Hudson Strait system is included. Results of this experiment, in comparison with observation, reveal the general behavior of our barotropic model. The remaining experiments are designed to determine the influence of individual factors. EXP2

is applied to the whole domain, but using pressure forcing only. EXP3 and EXP4 are run using the model domain excluding the Hudson Bay–Hudson Strait system, the former being driven by both forcings and the latter with atmospheric pressure forcing only. These two experiments are designed to determine the influence of the Hudson Bay Hudson Strait system on bottom pressure on the Labrador and Newfoundland Shelf. EXP2, EXP3 and EXP4 are run for one year. The model runs start from a state at rest. An test experiment shows that the results are independent of initial condition about two weeks after the model started.

Quadratic bottom friction with $k = 2.5 \times 10^{-3}$ and a horizontal eddy viscosity coefficient of $A_h = 10^3$ m^{2}s^{-1} are used in all of the above experiments. These values of k and A_h reproduce the right pattern of amphidromic points under tidal forcing, suggesting their appropriateness for our study. For models driven by monthly or seasonal mean wind fields, the currents will be weaker and thus cause a weaker damping. In that case, the linear form of the bottom friction is usually used (e.g.,GG). To test the sensitivity of the model to the bottom friction formulation, we make two short runs using the linear bottom friction law with $r = 5 \times 10^{-4} ms^{-1}$, one under both wind and atmospheric pressure forcings and the other under pressure forcing only. The results of the two tests are compared with those of EXP1 and EXP2 respectively.

Figs. 2.2-2.4 show that, for both wind and atmospheric pressure forcing, the

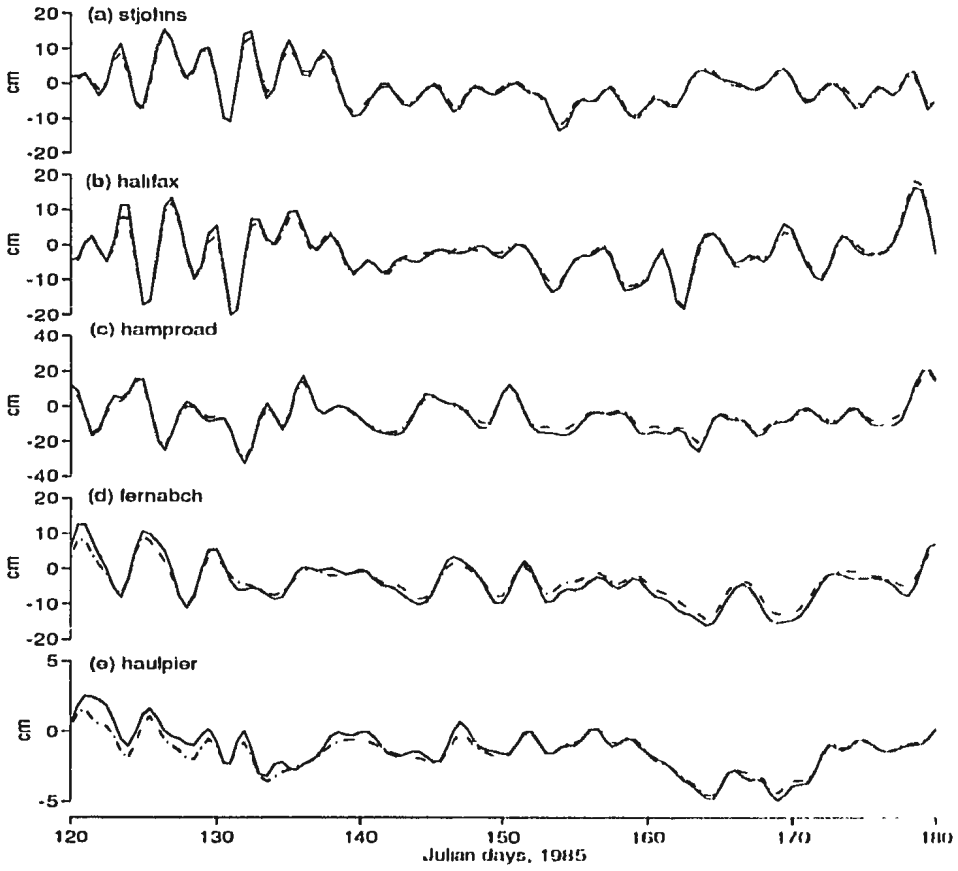

Figure 2.2: Adjusted sea level at 5 tide gauges along the western boundary, from models runs under both wind and atmospheric pressure forcing. Solid lines are from EXP1, using the quadratic bottom friction with $k = 2.5 \times 10^{-3}$. Dot-dashed lines are from the same model except that linear bottom friction with $r = 5 \times 10^{-4} ms^{-1}$ is used. Locations of the 5 gauges are shown in Fig. 3.1.

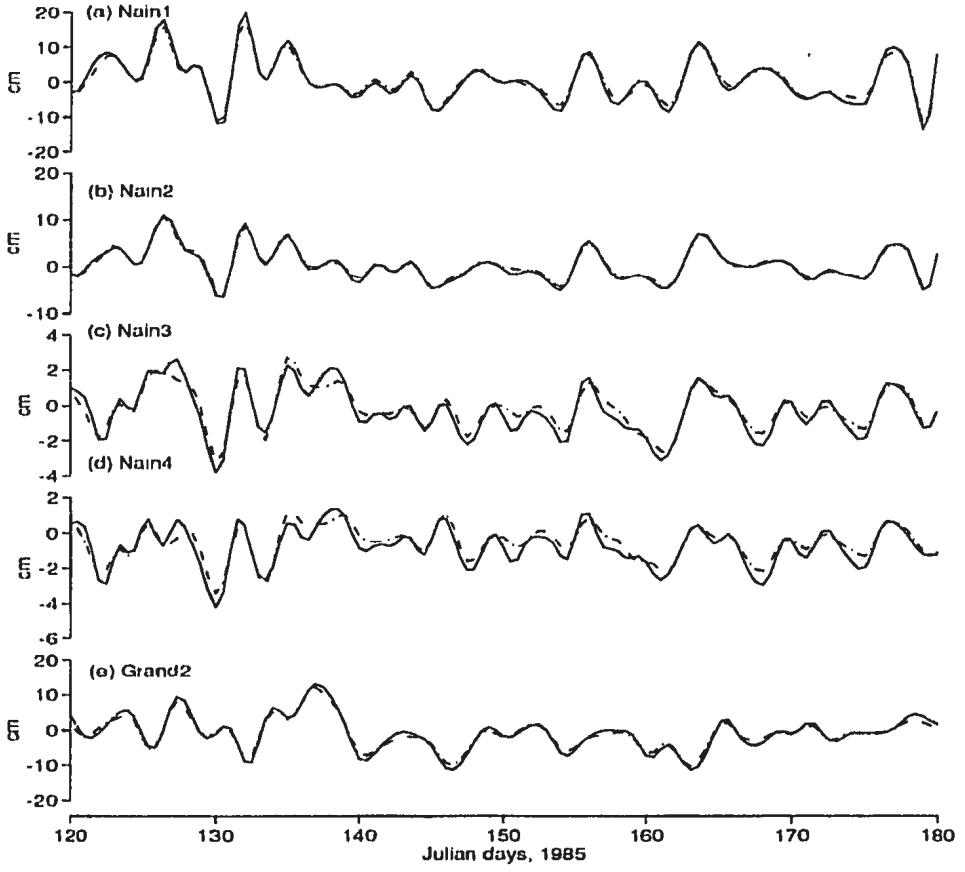

Figure 2.3: Same as Fig. 2.2 but at the location of 5 bottom pressure gauges on the Labrador and Newfoundland Shelf. Locations of the 5 gauges are shown in Fig. 5.1.

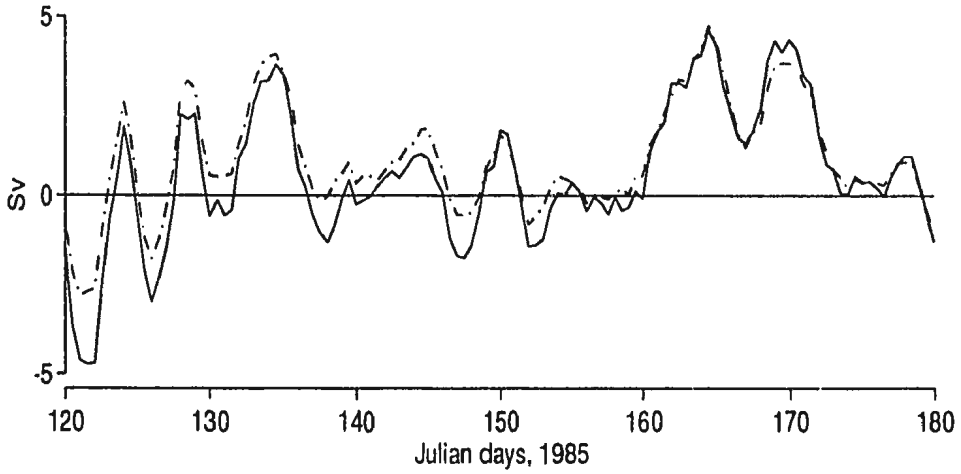

Figure 2.4: Same as Fig. 2.2 but for the volume transport through the Florida Straits.

model gives almost the same results using quadratic bottom friction with $k = 2.5 \times 10^{-3}$ as it does using linear bottom friction with $r = 5 \times 10^{-4} ms^{-1}$, at least as far as the along-coast and across-shelf adjusted sea level (and bottom pressure), as well as the volume transport through the Florida Straits is concerned. This means that, at least on the shelf and near the coast, our choice of quadratic bottom friction in the model runs to be described gives results comparable to those obtained using linear bottom friction with $r = 5 \times 10^{-4} ms^{-1}$. The latter corresponds to a damping time, $\frac{H}{r}$, of 4.6 days for a depth of 200m and 23 days for a depth of 1000m. Putting $k|\mathrm{u}| = r$ with $k = 2.5 \times 10^{-3}$ and $r = 5 \times 10^{-4} ms^{-1}$ gives $|\mathrm{u}| = 0.2 ms^{-1}$, a typical value obtained in the shelf regions for both cases.

We wish to study the contribution of "wind-only" from the above experiments.

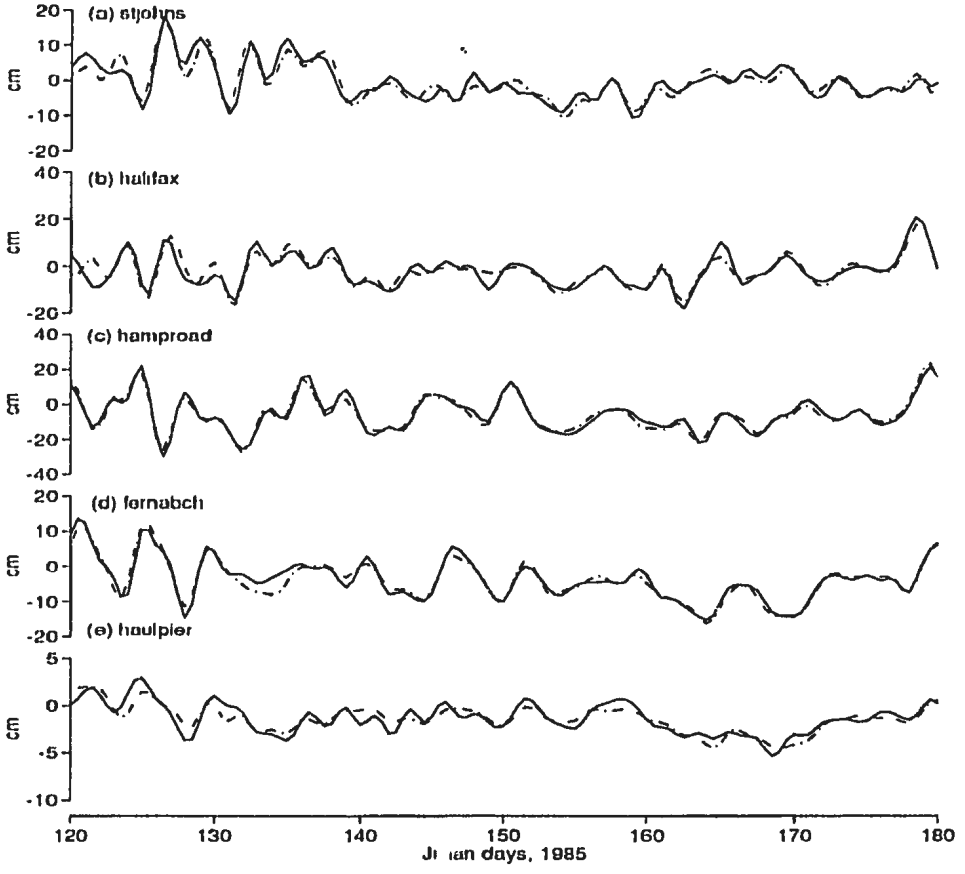

Figure 2.5: Adjusted sea level at 5 tide gauges along the western boundary. Solid lines are obtained by subtracting the results of EXP2 from EXP1. Dot-dashed lines are from a test driven by wind only, using the same quadratic bottom friction as in EXP1 and EXP2.

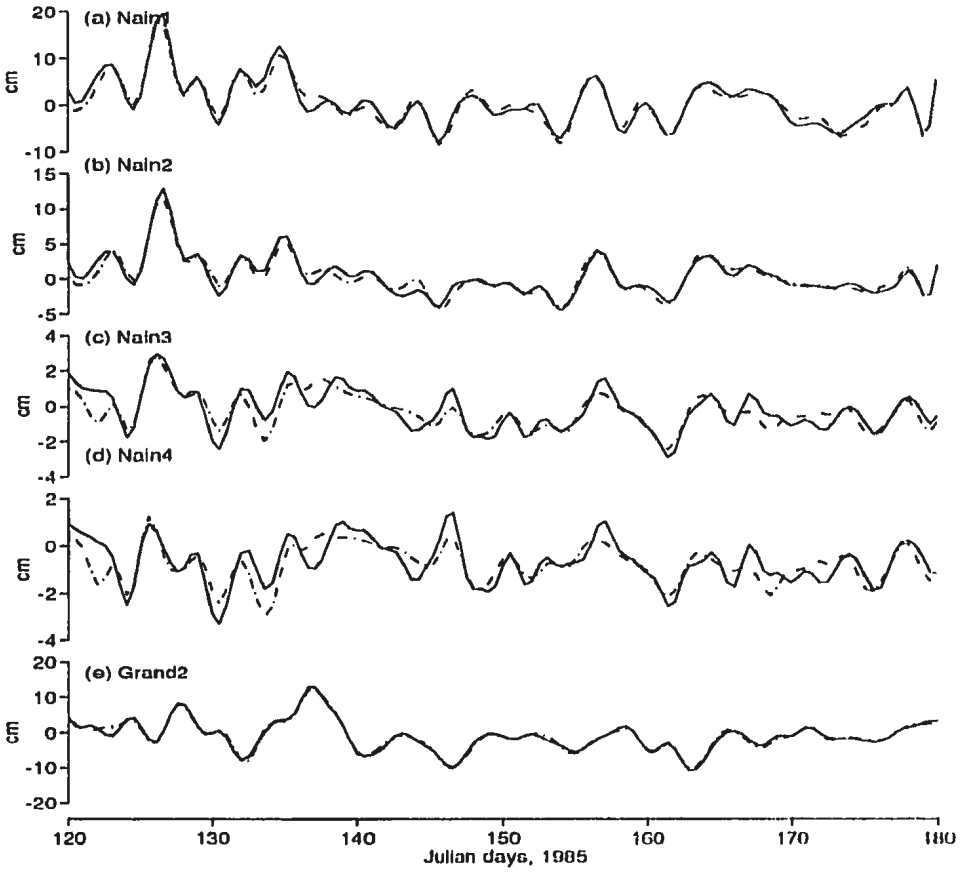

Figure 2.6: Same as Fig. 2.5 but at the location of bottom pressure gauges as in Fig. 2.3.

This is carried out, for the Hudson Bay–Hudson Strait system included case, by subtracting the results of EXP2 from EXP1; and for the Bay/Strait system excluded case, by subtracting the results of EXP4 from EXP3. The accuracy of this process is not guaranteed because of the use of quadratic bottom friction, but can be assessed from Figs. 2.5-2.6. These figures show that, for the Bay/Strait system included case, the adjusted sea level obtained by subtracting the results of EXP2 from EXP1 is in agreement with that obtained from a test experiment driven by wind forcing only, using the same quadratic bottom friction as in EXP1 and EXP2.

Chapter 3

Variations of Sea Level

3.1 Introduction

Sea level data have been collected at a greater number of stations and over longer periods than most other observations for the ocean. Interpreting these data provides one means to understand the variability in the ocean. An example (Maul et al., 1990) is the attempt to infer variations of the Florida Current from the sea level observed at nearby tide gauges, particularly because long-period transport measurements were unavailable before the advent of the cable data (Larsen, 1992).

Sea level variations can be attributed to wind and atmospheric pressure forcing, large scale ocean current and thermohaline changes. Blaha (1984) analyzed the

monthly sea level fluctuations observed in the South Atlantic Bight (from Key West to Norfolk). The effect of atmospheric pressure was treated as an inverse barometer. Local heating and cooling at the sea surface results in an annual cycle of steric sea level within the upper layer of water. Contributions from the local winds were determined by a multiple regression method. These three effects were removed from the observed sea level time series. The residual component was investigated for its relationship to the fluctuations of the Gulf Stream. It was found that the seasonal sea level signal in and to the north of the Florida Straits appears similar to that observed in the Caribbean and Gulf of Mexico, suggesting a common underlying driving mechanism in these regions.

A study of the monthly mean sea level from an extensive array of tide gauges along the coast of the North Atlantic was provided by Thompson (1986). The spatial scale of sea level change was found to be large. Coherent signals were found within three distinct groupings of tide gauges: one located on the eastern boundary and on the western boundary two groups, respectively north and south of Cape Hatteras. A regression method similar to that of Blaha (1984) was applied to determine the effects of local winds and seasonal cycles. Sea level variation along the eastern boundary was found to be related to changes in the flat-bottomed Sverdrup transport of the North Atlantic and hence the large-scale wind field, the correlation between the two

increasing with decreasing frequency. At the western boundary, it was speculated that changes in the Gulf Stream would have contributions.

As mentioned in Chapter 1, GG's results from a coarse resolution ($1^\circ \times 1^\circ$) North Atlantic model forced by monthly mean seasonal wind stresses achieved some success in explaining the part of seasonal sea level variation caused by wind forcing. Follow-up studies of Greatbatch et al. (1990) and de Young et al. (1992) with fine-resolution models investigated the variability on the Labrador and Newfoundland Shelf, at seasonal and synoptic time scales, respectively. These models were solved in frequency domain and thus preventing a statistical study over a wide frequency band. The use of the rigid-lid approximation made these models inappropriate to study the non-isostatic response to atmospheric pressure. These shortcomings are overcome in the present study.

3.2 Model Results

Model-calculated sea level is compared with observations at 15 tide ganges, situated around the North Atlantic. Locations of these stations are listed in Table 3.1 and shown in Fig. 3.1. Observations from these stations, sampled at 6-hour intervals, were obtained from the Marine Environmental Data Service. Harmonic analysis is

Table 3.1: List of tide gauges where model output of sea level is compared with observations. Locations are shown in Fig. 3.1.

#	Station	Latitude (°N)	Longitude (°W)
1	St. John's, NF	47.57	52.68
2	Halifax, N.S.	44.38	63.35
3	Portland, ME	43.41	70.18
4	Atlantic City, NJ	39.21	74.29
5	Hampton Roads, VA	37.02	76.23
6	Charleston, SC	32.48	79.58
7	Fort Pulaski, GA	32.03	80.54
8	Fernandina Beach, FL	30.30	81.26
9	Haulover Pier, FL	25.75	80.25
10	Reykjavik, Iceland	64.09	21.58
11	Newlyn, Britain	50.06	5.34
12	Brest, France	49.23	4.30
13	La Coruna, Spain	43.22	8.24
14	Lagos, Portugal	37.05	8.40
15	Las Palmas, Spain	28.08	15.27

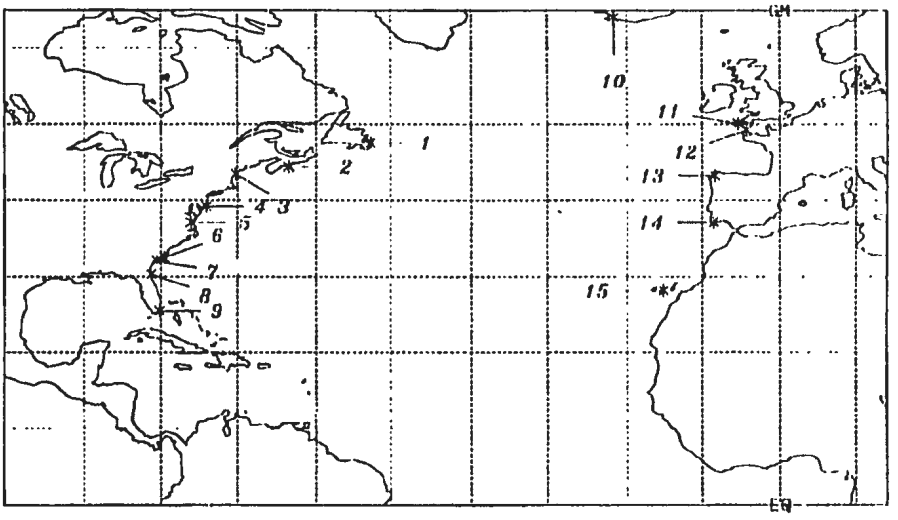

Figure 3.1: Locations of tide gauges along the coast as listed in Table 3.1

performed on each record to remove the dominant tidal signals. A low-pass filter with cutoff at 32 hours is applied to the data to remove any residual energy below 1 cycle per day. The IB response of sea level, calculated by taking the average of atmospheric pressure over a global ocean domain, is then removed to obtain the adjusted sea level for observational data.

As stated in Chapter 2, the IB response of model-calculated sea level is calculated by taking the average of p_a over the model domain. This is removed from the model output of sea level fields to extract the time series of adjusted sea level at these gauges. A low-pass filter with cutoff at 1.5 days is performed on the modeled time series for comparison with observations.

Time series of adjusted sea level obtained from observation and our primary model experiment, EXP1, are plotted in Figs. 3.2 and 3.3, for 1-year duration from July 1985 to June 1986. Agreement between model and observation is found at all the gauges at the western boundary except Haulover Pier (Miami). At the eastern boundary, there is little agreement, except perhaps at Newlyn and Brest. Failure of the model to reproduce the observations at Reykjavik may be attributed to our unrealistically closed northern boundary which passes through Iceland. The reason for the disagreement at Haulover Pier, La Coruna, Lagos and Las Palmas needs to be explored. We shall return to this in the next section.

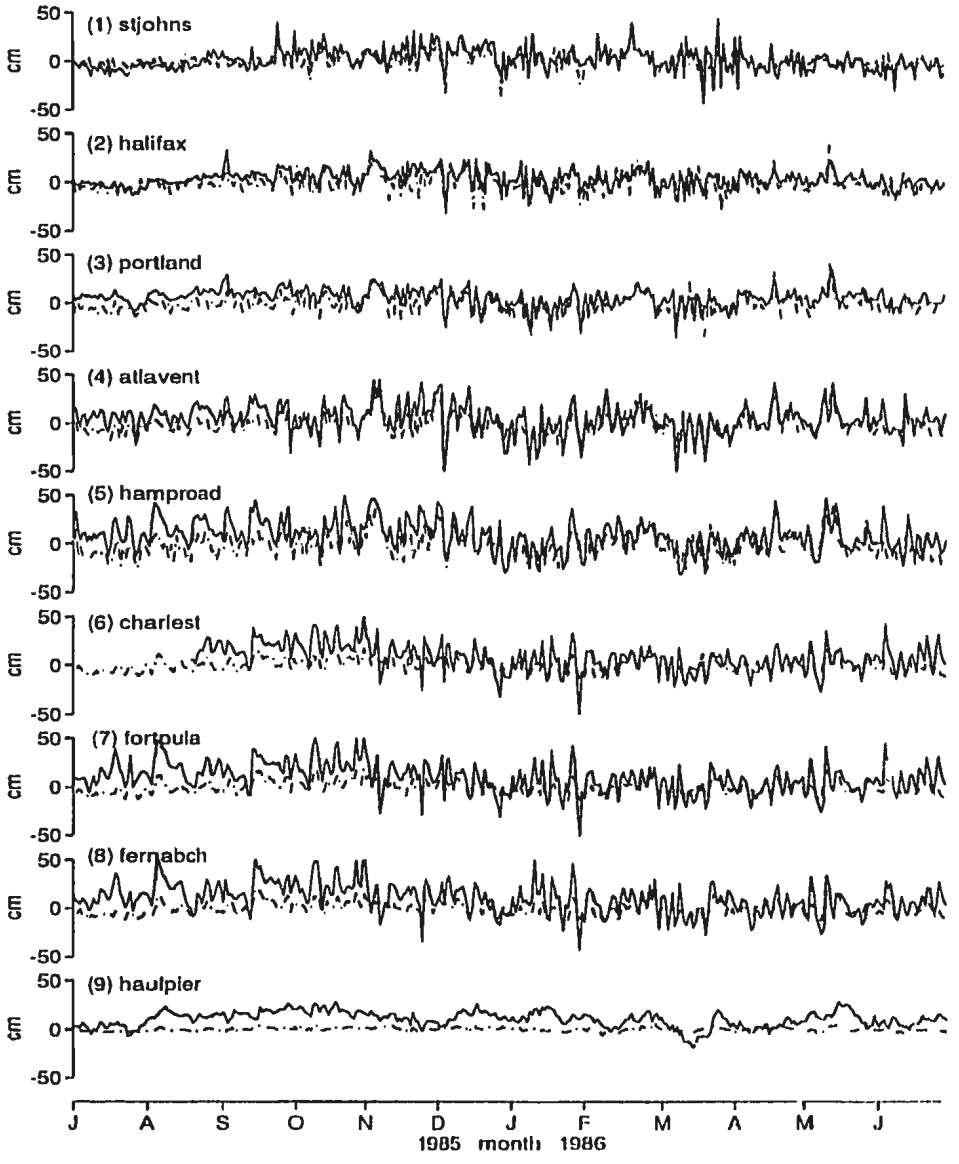

Figure 3.2: Time series of adjusted sea level for tide gauges along the western boundary, for 1-year duration from July 1, 1985 to 30 June, 1986. Solid lines are from observation and dot-dashed lines are from EXP1. The number before the station name corresponds to the station number shown in Fig. 3.1.

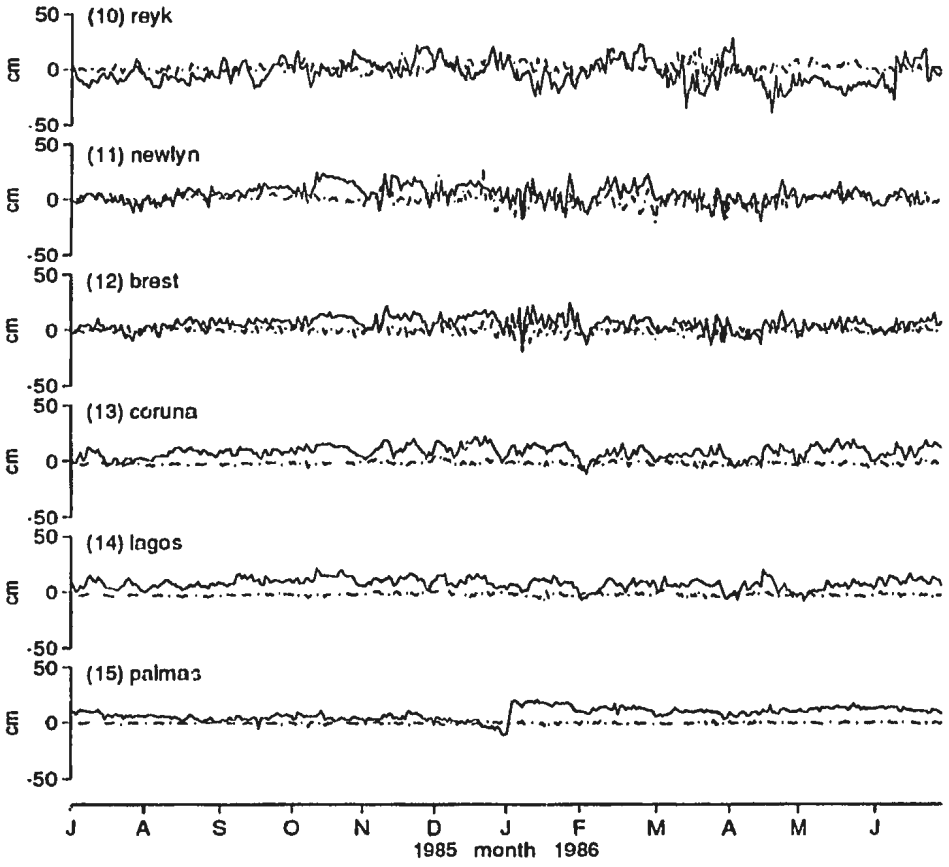

Figure 3.3: Same as Fig. 3.2 but for tide gauges along the eastern boundary.

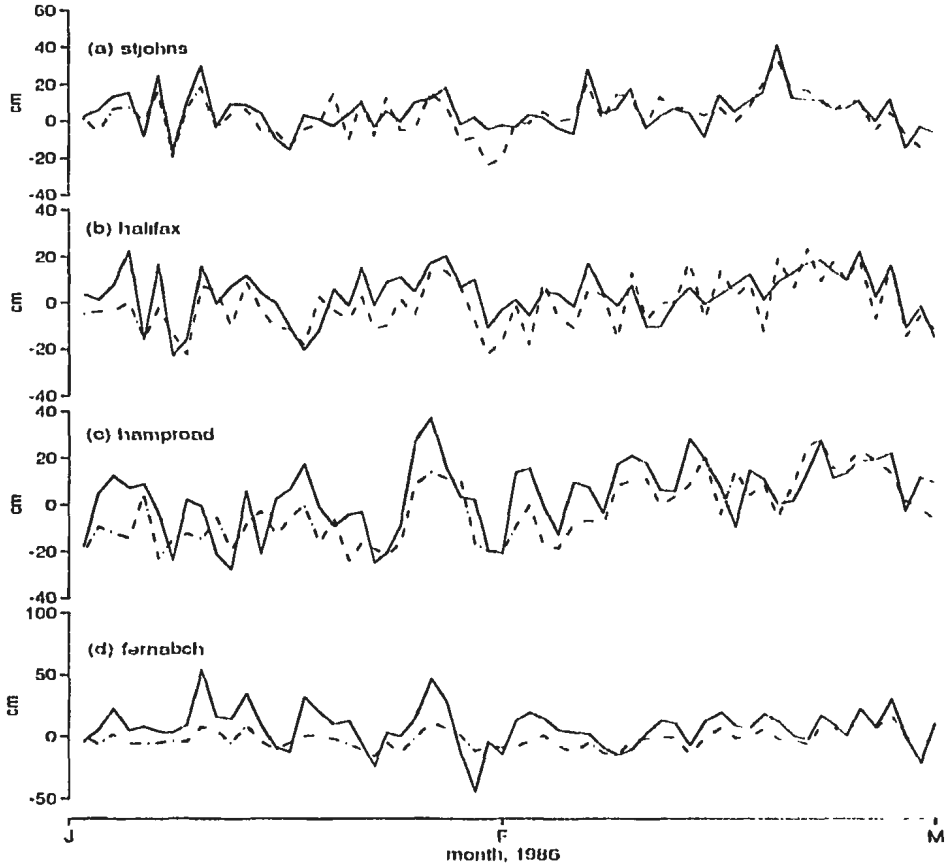

Figure 3.4: An expanded view of Fig. 3.2 for the first 2 month of 1986 at 4 stations along the western boundary. Solid lines are from observations and dot-dashed lines from EXP1.

To examine the behavior of the model at stations where good agreement between model and observation is found, we chose four stations along the western boundary, namely St. John's, Halifax, Hampton Roads and Fernandina Beach. These stations are representative of the Grand Banks of Newfoundland, the Scotian Shelf, the Middle Atlantic Bight (north of Cape Hatteras) and the South Atlantic Bight (south of Cape Hatteras), respectively. The behavior of the model at short periods is illustrated in Fig. 3.4, an expanded view of Fig. 3.2 for the first two months of 1986. Short-period events (about several days) are well captured by the model. The model is quite in phase with observation at all the four stations and estimates the right amplitude of variation at the three northern stations, but underestimates the amplitude at Fernandina Beach.

Statistical analysis is performed at the four stations selected above. Coherence between observation and EXP1 is well above the 95% confidence level for all the four stations at periods beyond 3 days and the model results are in phase with observation (Fig. 3.5). The coherence peaks shift from ~3-8 days at Fernandina Beach to ~5-15 days at Hampton Roads. A drop in coherence is found at ~12 days at Fernandina Beach.

Power spectral density and variance conserving spectra plots (Figs. 3.6 and 3.7) show that EXP1 gives a similar trend of energy distribution with that of observation at

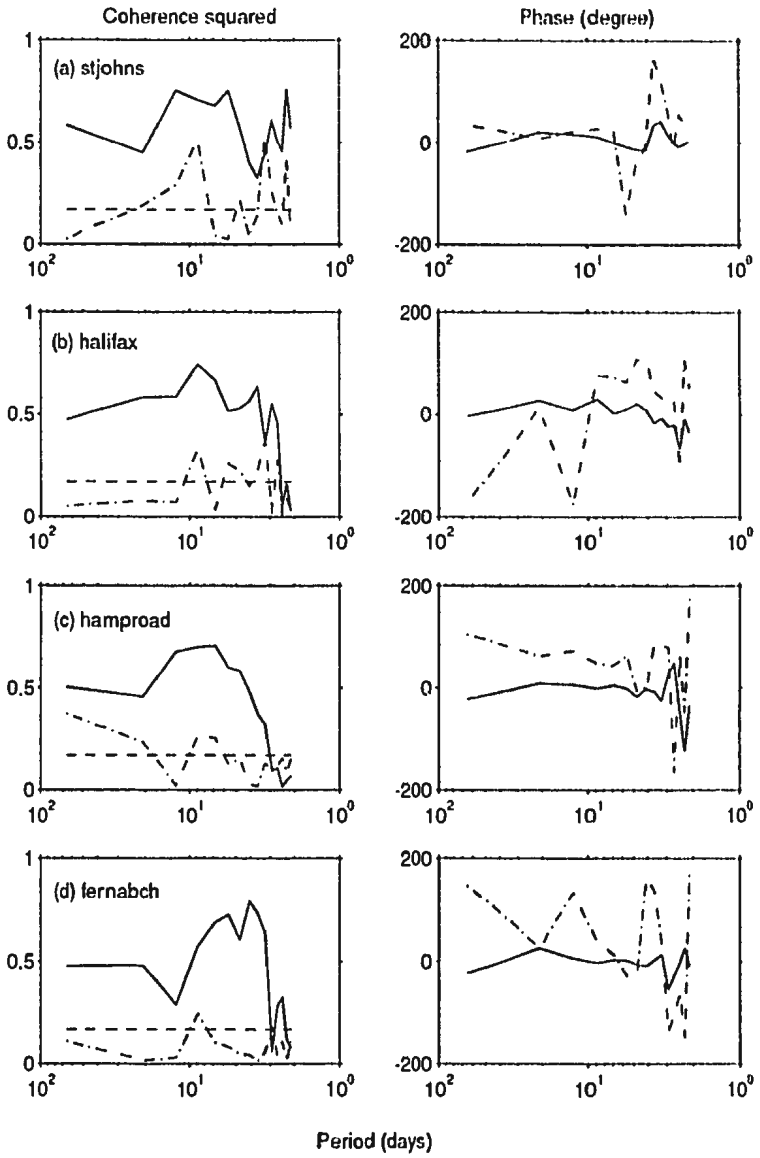

Figure 3.5: Coherence squared and phase lag between observed and model-calculated adjusted sea level, at 4 stations at the western boundary. Solid curves are observation vs. EXP1; dot-dashed curves are observation vs. EXP2. Coherence above the horizontal dashed lines is significant at the 95% level. Positive phase means that observations lead model.

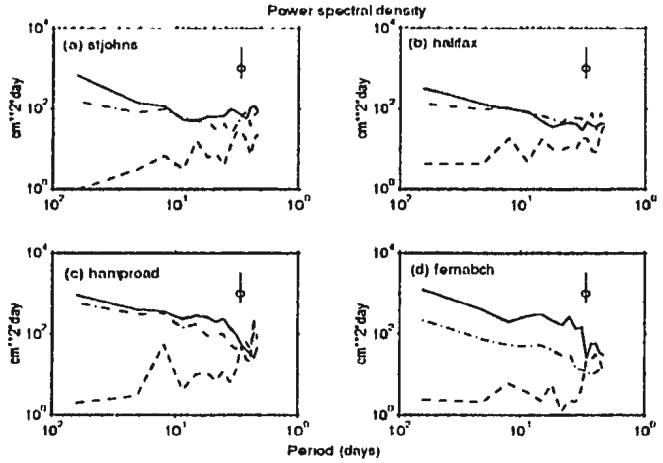

Figure 3.6: Power spectral density spectra of adjusted sea level at 4 stations as in Fig. 3.5. Solid lines are from observation, dot-dashed lines from EXP1, and dashed lines from EXP2. The 95% confidence error bars are shown in the upper right corner.

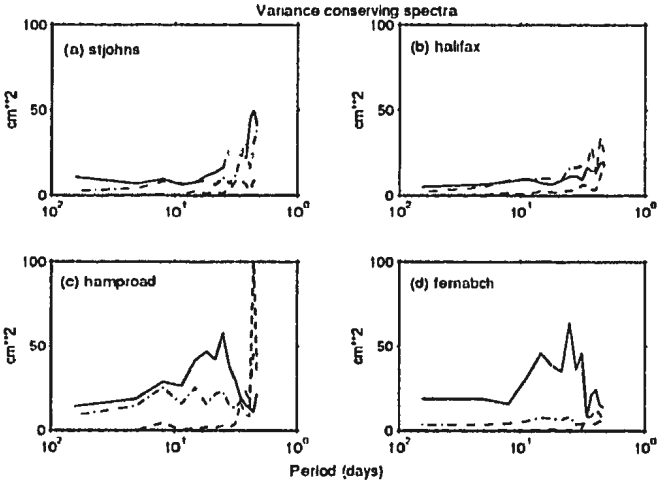

Figure 3.7: Variance conserving spectra corresponding to Fig. 3.6.

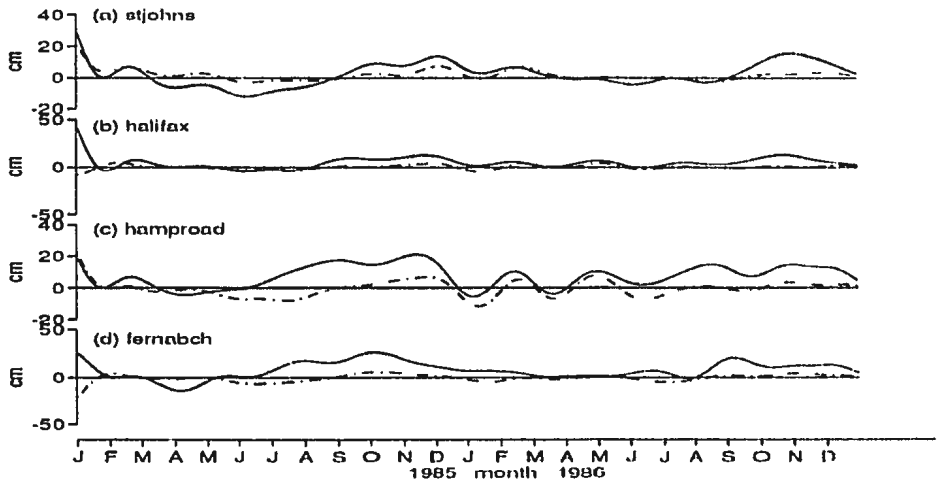

Figure 3.8: 2-year (1985-1986) time series of adjusted sea level at 4 stations along the western boundary, after performing a low-passed filter with a cutoff period of 60 days. Solid lines are from observation and dot-dashed lines from EXP1.

the four stations. Energetic peaks at periods below 20 days are generally reproduced, but the model underestimates the energy for the two southern stations. Another feature is that the model underestimates the energy density at periods beyond 30 days, for all of the four stations.

The inability of the model to capture the longer time scale variability of adjusted sea level can be illustrated more clearly by performing a low-passed filter with a cutoff period of 60 days to both the observed and modeled time series (Fig. 3.8). Although the model captures some of the variation at periods of several months, discrepancies between model and observation at longer time scales are evident. The model underestimates the amplitude of variation at seasonal time scales in the obser-

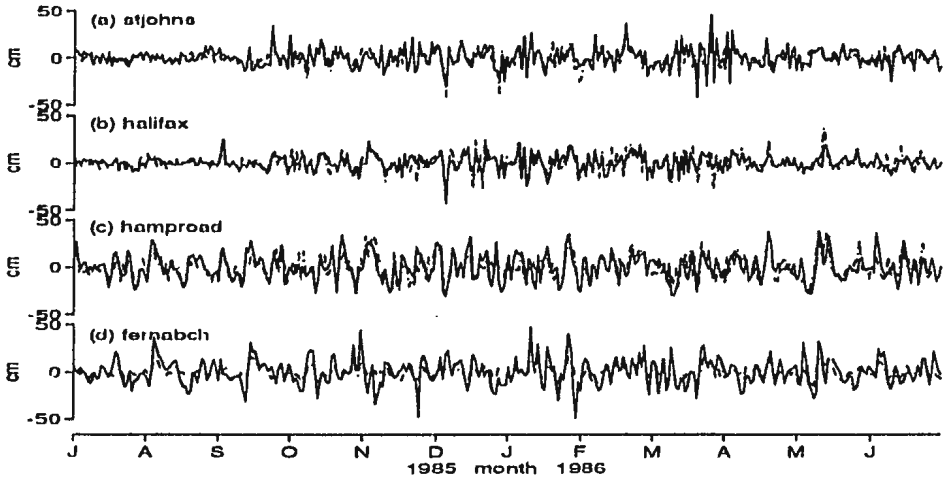

Figure 3.9: Time series of adjusted sea level at 4 stations along the western boundary, after performing a high-passed filter with a cutoff period of 60 days, for 1-year duration from July 1, 1985 to June 30, 1986. Solid lines are from observation and dot-dashed lines from EXP1.

vation, except at Halifax, where the variation at seasonal time scales is rather weak. A major contribution to seasonal variation in sea level, as we know, comes from the steric effect, a process not included in our model. The weak seasonal variation in the observational data of Halifax corresponds to a weak steric response there, as suggested by Thompson (1986). In contrast to the situation at long time scales, performing a corresponding high-passed filter clearly shows that the model behaves best at shorter time scales, especially to the north of Cape Hatteras (Fig. 3.9).

The contribution from the atmospheric pressure forcing to adjusted sea level is demonstrated by the results of EXP2, as shown in Fig. 3.10. Comparing with

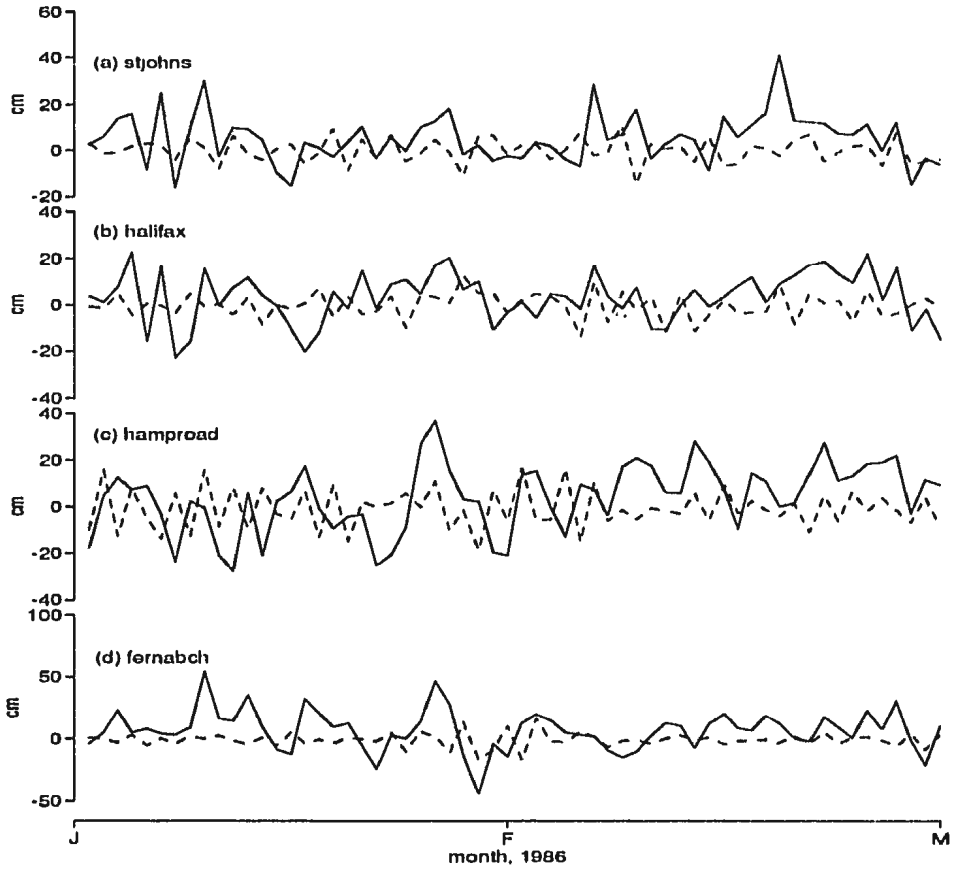

Figure 3.10: Time series of adjusted sea level in the first 2 month of 1986 at 4 stations at the western boundary. Solid lines are from observation and dot-dashed lines are from EXP2.

Fig. 3.4, it is clear that EXP1 gives better agreement with observation. Statistical analysis (Figs. 3.5-3.7) shows that coherence peaks above the 95% confidence level at periods below 3 days, and that the energy density increases with decreasing time scales. Power spectral density and variance conserving spectra plots (Figs. 3.6 and 3.7) demonstrate the general trend that the atmospheric pressure driven non-isostatic response becomes increasingly significant as frequency increases. This is consistent with the conclusion of Ponte et al. (1991), who found that the non-isostatic effect dominates the IB response at periods shorter than ~2-3 days. Our analysis does not resolve periods shorter than two days.

3.3 Discussion

The agreement between modeled and observed adjusted sea level varies with location and time scale. This provides clues to investigate the essential physics determining the observations.

First it is evident that all the gauges where good agreement is obtained are at coastal locations with broad shelves, whereas stations showing poor agreement have narrow shelves offshore (Figs. 2.1 and 3.1). The immediate conclusion is that the model can well reproduce the sea level variation on broad shelves. As our model is

purely barotropic, this result is consistent with the argument of Huthance (1992), that on a shelf with width $L > NH/f$ (where N is the buoyancy frequency, H the water depth, and f the Coriolis parameter), stratification effects tend to be weak and the sea level responses are dominated by the barotropic Kelvin wave and the gravest mode of coastal trapped waves. Typical values of $N \sim 0.05s^{-1}$ and $H \sim 200m$ give $L > 100km$. Clearly poor agreement is obtained at stations located on shelves narrower than this width.

The effects of stratification in shelf regions may take the form of baroclinic Kelvin waves. Pares-Sierra and O'Brien (1989) showed that an $1\frac{1}{2}$ layer model can capture the features of sea level variation at seasonal and interannual time scales, along the eastern boundary of the North Pacific. They argued that the baroclinic Kelvin waves would combine with the topographic Rossby waves along the eastern boundary, thus the hybrid (part Kelvin and part shelf) wave activity should be relevant. In fact, the theory of hybrid waves (Clarke, 1977; Wang and Mooers, 1976; etc.) has been successfully used in explaining the character of wind-forced variability at shorter time scales (hours and days) (see e.g., Battisti and Hickey, 1984).

A weakness in the present model is that advection by the mean flow has not been included. Mean flow can carry information downstream and thus distort the response. Greatbatch and Li (1990) showed, using a barotropic vorticity equation

model applied to an idealized domain, that this influence might be significant near the western boundary and in the inertial recirculation region. Thus the mean flow of the Loop Current/Florida Current system might play a role in communicating the wind-field variation in the Caribbean and Gulf of Mexico northward to the Florida Straits. This might be responsible for the drop of coherence at ~12 days at Fernandina Beach. Similar influence might exist in other regions. For example, the Labrador Current might influence the sea level response at St. John's.

The steric effect, which has not been removed from the observational data, may cause the discrepancy found at seasonal time scales. The least discrepancy is obtained at Halifax, where the amplitude of the steric response is almost zero (Thompson, 1986). In studying the seasonal cycle of sea level variations with barotropic models, a proper correction of steric effect must be performed (see GG).

As mentioned earlier, the contribution of wind forcing comes from local set-up as well as large-scale circulation. At the western boundary, results from regression analysis (Blaha, 1984; Thompson, 1986) have revealed that local winds exhibit significant contribution to sea level variation at all tide gauges except Miami. We would therefore conclude that our model can reproduce the contribution from the local winds, especially on the broad shelves, as our model grid-spacing of ~37 km at midlatitude could not resolve the topographic variation on shelves narrower than this. At the

western boundary, the influence from the Gulf Stream is expected to be important, particularly to the south of Cape Hatteras. In the next chapter we shall examine the ability of the model in reproducing the volume transport through the Florida Straits.

Chapter 4

Variations of Transport Through the Florida Straits

4.1 Introduction

Volume transport through the Florida Straits has been measured by several methods. The Florida Current, which passes through the Straits, carries on average about 30 Sv of water (Niiler and Richardson, 1973; Larsen, 1992) directly into the Gulf Stream. Monitoring the current is therefore an important measure of climate variability in the North Atlantic region (Molinari et al., 1985). A time series of the transport, with time scales ranging from subtidal to interannual, has been derived from voltage

measurements using a submarine cable under the current at 27°N (Larsen,1992). Reproducing the variability in this time series provides a stringent test for any North Atlantic circulation model, as noted by Böning et al. (1991).

There have been a number of studies on the seasonal cycle of transport using numerical models (Anderson and Corry, 1985; Fanning et al., 1994; GG). These models are all at a resolution of $1^{o} \times 1^{o}$ and are forced by monthly mean seasonal varying wind stress fields and incorporate the realistic topography of the North Atlantic. Anderson and Corry (1985) presented the results from both a two-density-layer model and a single-layer barotropic model. The important conclusion is that below annual time scales, most of the response in their baroclinic model can be captured by a uniform density, barotropic version of the model. The work of GG and Fanning et al. (1994) with linear barotropic models produced similar seasonal cycles to that of Anderson and Corry's. Fanning et al. (1994) compared the responses using different wind stress climatologies and showed that the seasonal cycle calculated depends strongly on the wind stress climatology used to drive the model.

The relevance of wind forcing to the variation of transport through the Florida Straits, at periods from days to seasonal, is addressed by Schott et al. (1988) and Lee and Williams (1988, hereinafter LW). Schott et al. (1988) noted the similarity in the annual cycle of transport to that of the along-channel wind stress component within

the Straits and the wind stress curl in the vicinity. At periods below seasonal, a simple dissipation model could account for the portion of transport variability coherent with along-channel wind forcing (Schott et al., 1988). LW showed that a wind-forced channel model can provide a good estimation of the observed transport variation at synoptic time scales of ~4-10 days. This analysis was for the winter period from 1 December 1983 to 1 March 1984. LW also found that, for a 2-year period from 9 April 1982 to 9 April 1984, this simple model could estimate the seasonal changes in observed transport. However, they have to use a different integration time scale, an empirical parameter in their calculation, to capture the variability at different periods. LW argued that this might be related to the differences in the time and spatial scales of the relevant wind forcing. A numerical model with a sufficiently large model domain should avoid the arbitrary choice of the integration time scale. The above studies provide encouragement for further investigation of volume transport variations through the Florida Straits with a barotropic model under realistic wind forcing.

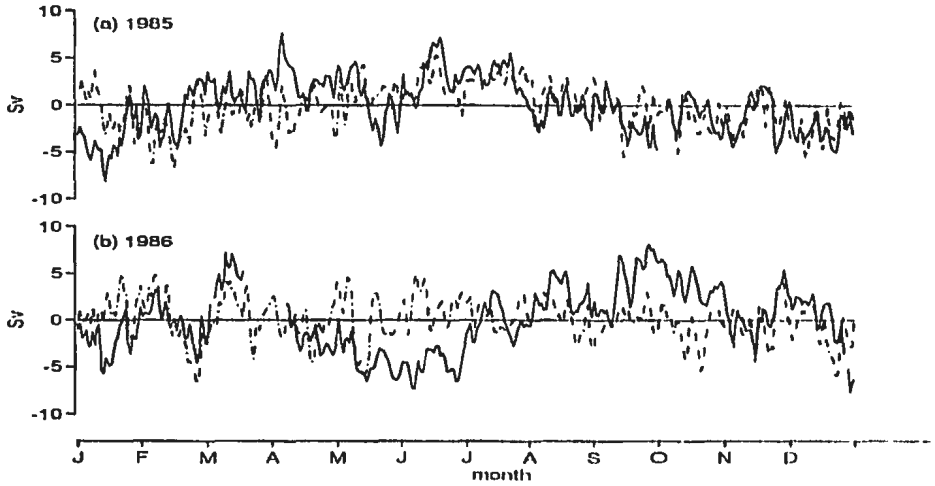

Figure 4.1: De-meaned volume transport variation through the Florida Straits at 27°N, for (a) 1985 and (b) 1986. Solid lines are cable data of Larsen (1992), dot-dashed lines are from EXP1.

4.2 Model Results

Two-year (1985-1986) time series of de-meaned volume transport through the Florida Straits at 27°N, both from the cable data of Larsen (1992) and EXP1, are presented in Fig. 4.1. The cable data are daily means corrected for tides and geomagnetic noise. A low-pass filter with a cutoff period of 1 day is applied to the model-calculated time series to remove the energy below 1 day. Better agreement between model output and observation is found in 1985 than in 1986. The model does quite well in capturing the short period (of several days) variation features in both years. This can be seen more clearly by applying a high-pass filter with cutoff period of 60 days to the above

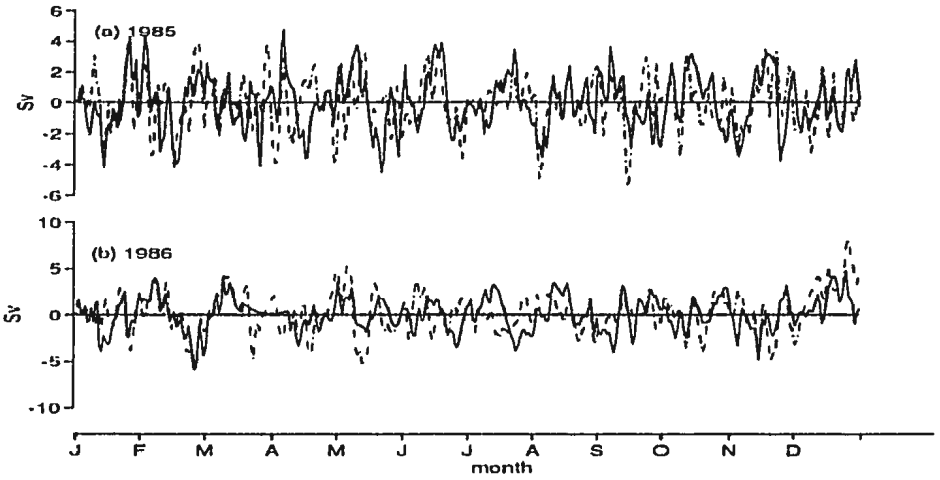

Figure 4.2: High-frequency variation of volume transport obtained by performing a high-pass filter with cutoff period of 60 days to the time series shown in Fig. 4.1. Solid lines are cable data and dot-dashed lines are from EXP1.

time series, as shown in Fig. 4.2. The model does well at estimating the amplitude of variation in the cable data, and the two are generally in phase.

The model shows less ability to estimate the long time scale (several months to seasonal) variation in the cable data, as can be seen from Fig. 4.1, or more clearly, by applying a low-pass filter with cutoff period of 60 days to both the observed and modeled time series (Fig. 4.3). Greater discrepancies are found in 1986 than in 1985. In 1985, a signal at seasonal time scale is present in the observations, and it is captured, to some extent, by the model. In 1986, the long time scale variation is missed by the model. As can be seen in Figs. 24 and 25 of Larsen (1992), the long time scale variation in 1985 is closer to the mean seasonal cycle obtained by averaging

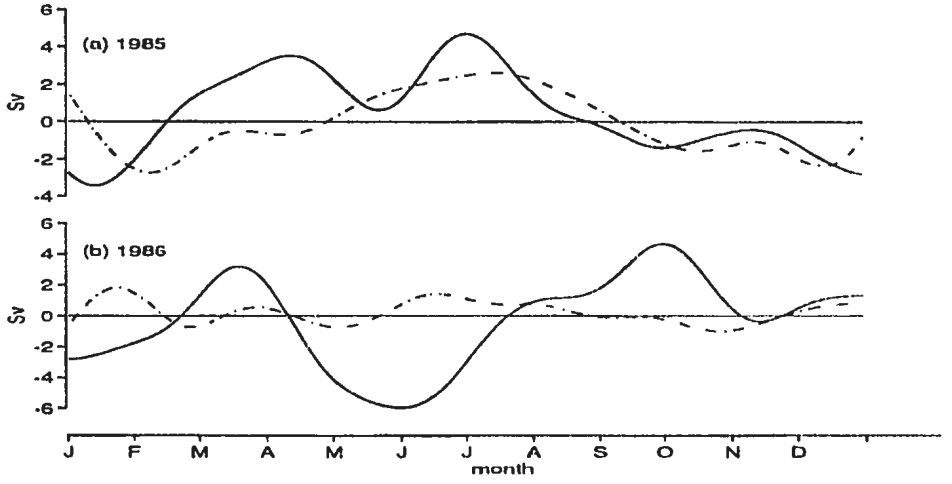

Figure 4.3: Low-frequency variation of volume transport obtained by performing a low-pass filter with cutoff period of 60 days to the time series shown in Fig. 4.1. Solid lines are cable data and dot-dashed lines are from EXP1.

over the nine-year period of 1981-1990, but this is not true in 1986. A two-year time series is, however, not long enough to get the mean seasonal cycle.

Statistical analysis (Fig. 4.4) shows that, significant coherence is obtained at periods beyond 3 days in 1985, in the range of 3-50 days in 1986 as well as for the two-year analysis. A drop in the coherence, either for the two-year analysis or for each year individually, occurs at $\sim$10 days. Coherence peaks significantly above the 95% confidence level are obtained at the period range of 3-8 days. LW's simple channel model produced similar results. The best agreement between their model and observation was obtained in winter with strong along-channel wind forcing, with highest coherence in the period band of 4-10 days. Our model behaves moderately

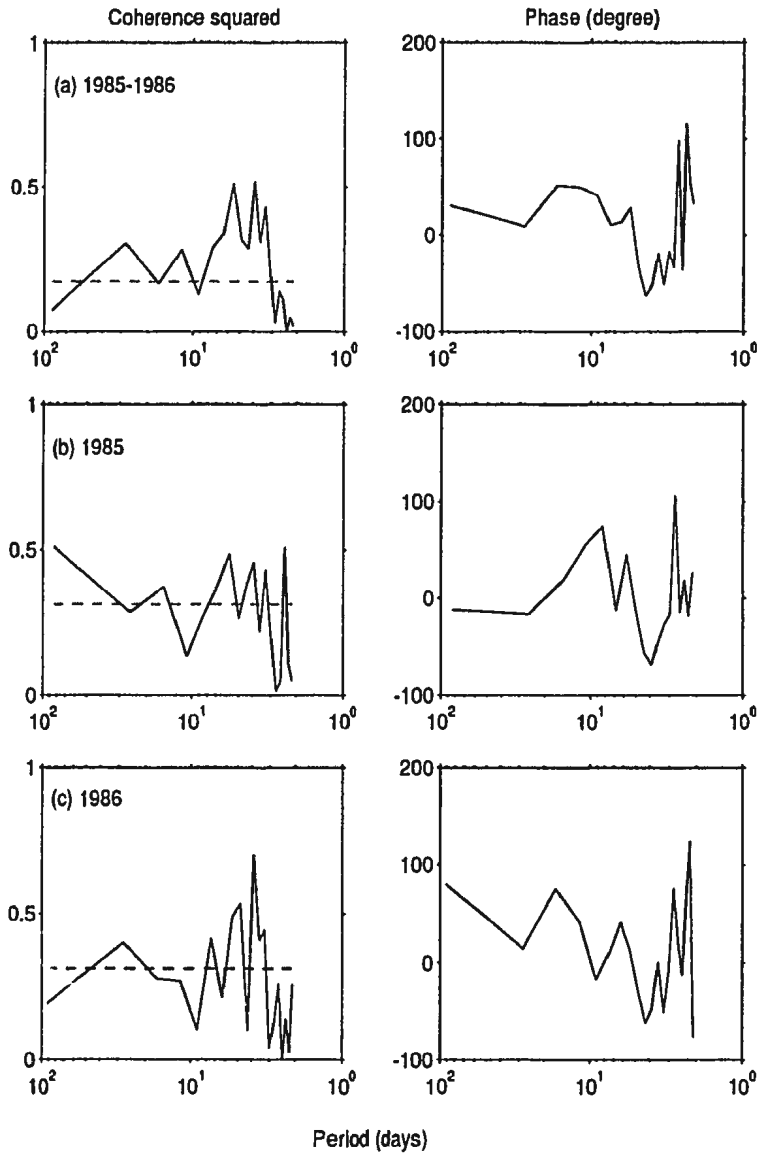

Figure 4.4: Coherence squared and phase lag between observed and modeled volume transport. (a) is for the two-year duration of 1985-1986, (b) and (c) are for 1985 and 1986 separately. Coherence above the dashed lines is significant at the 95% level. Positive phase means observation leads model.

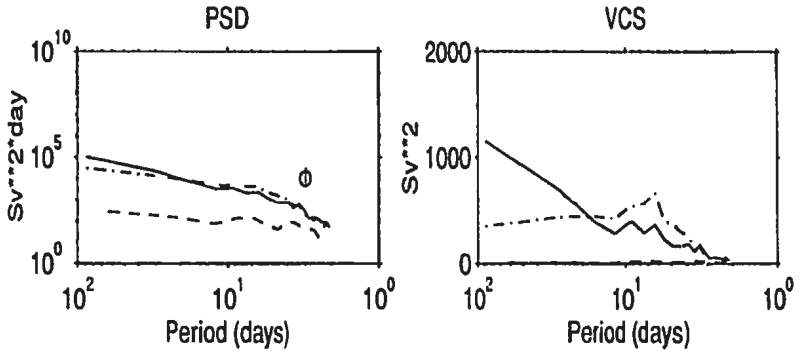

Figure 4.5: (a) Power spectral density spectra and (b) variance conserving spectra of volume transport through the Florida Straits. Solid line are for cable data, dot-dashed lines for EXP1, and dashed lines for EXP2. The 95% confidence error bars for power spectra estimation are shown at the upper right corner of (a).

well throughout the year (coherence squared ~0.3-0.4), in capturing the short time scale variation (as shown in Figs. 4.1 and 4.2.). Significant coherence obtained at periods of 20-50 days, for the two-year analysis, indicates that our model does better than LW's channel-model did in this period range. It should be noted that their empirical choice of integration period is avoided in the present numerical model.

Power spectral density and variance conserving spectra plots (Fig. 4.5) show that EXP1 produces a similar trend of power spectral density distribution as the observations, but overestimates the variance in the period range ~4-15 days, and un-

derestimates the variance beyond 20 days. Results from the model under atmospheric pressure forcing only (EXP2) show that the pressure forcing has negligible influence on the variation of volume transport through the Florida Straits in our model.

4.3 Discussion

One conclusion to be drawn from these results is that some of the variation of the Florida Current transport at synoptic scale can be explained by barotropic dynamics and attributed mainly to wind forcing. We did not separate the effect of local wind from the remote effect, but the agreement of our model behavior with that of LW's at this time scale indicates the local wind effect should be more relevant. Remote wind forcing may also be important, particularly at longer time scales. In modeling the seasonal cycle with monthly mean seasonally varying wind fields, previous barotropic model studies showed that winds north of 35°N (Fanning et al. 1994), or even north of 50°N (GG), play a role at Florida Straits. However, results from the Kiel version of WOCE-CME model found winds north of 35°N have little influence (Böning et al., 1991), suggesting the influence of processes not captured by the linear barotropic dynamics.

As mentioned at Chapter 3, the mean flow of the Loop Current/Florida Current

system might play a role in communicating the wind-field variation in the Caribbean and Gulf of Mexico northward to the Florida Straits. Excluding this effect in the present model might be responsible for the drop of coherence at periods ~10 days. In fact, comparing the coherence of volume transport (Fig. 4.4) and that of sea level at Fernandina Beach (Fig. 3.5), one notes that the two are quite similar. Further work incorporating the advection by the mean flow, such as that obtained from the large-scale eddy-resolving general circulation model (e.g., Holland and Bryan, 1989), is required to clarify this subject.

Problems remain as to variability at long time scales. The great difference in the cable data at long time scales between 1985 and 1986 (Fig. 4.3) indicates strong year to year variability. It seems likely this is associated with baroclinic dynamics not included in our model. However, it is intriguing to understand what causes the dramatic change in the Florida Current in 1986.

Previous studies of Anderson and Corry (1985), GG and Fanning et al. (1994) showed that the barotropic models could well capture the phase of the mean seasonal cycle although underestimate the amplitude. As strong year to year variation exists, two-year's calculation is not long enough to get the mean seasonal cycle. Model runs covering other years (for which we have cable data) are called for to further investigate this point.

Chapter 5

Variations of Bottom Pressure on the Labrador and Newfoundland Shelf

5.1 Introduction

The sea level analysis at St. John's in Chapter 3 provides evidence that the barotropic model could explain the observed sea level variability on Labrador and Newfoundland Shelf. We can investigate the response in this region by comparing model results with a bottom pressure dataset collected on the shelf (Wright et al.,1988).

Previous studies on the variability on the Labrador and Newfoundland Shelf, both from empirical regression analysis and numerical modeling, have revealed the basic dynamic features, but some inconclusive aspects still remain. At the seasonal time scale, wind forcing contributes a major part to the non-isostatic variation of sea level, as found by Thompson et al. (1986) from an empirical regression analysis of sea level at Nain, Labrador, and by Greatbatch et al. (1990, hereinafter GDGC) using a fine-resolution numerical model of the Shelf driven by the seasonally varying wind stress field of Hellerman and Rosenstein (1983). GDGC incorporated the influence of the North Atlantic wind forcing from the coarse resolution model of GC and found that this influence drives a significant part of the sea level variation on the Labrador Shelf.

Interesting questions remain at synoptic time scales. Garrett et al. (1985) used an empirical regression analysis to show that the response of sea level at Nain to atmospheric pressure forcing is significantly non-isostatic in the period range of ~2-10 days, which can not be explained by simple dynamical models. This result motivated the work of Wright et al. (1987), who argued that the non-isostatic response was due to a Helmholtz-like resonance response as the Hudson Bay-Hudson Strait system adjusts to variations in atmospheric pressure. Wright et al. used an analytical model as well as a crude numerical model to demonstrate this effect, and showed that it

might be significant in the period range ~2-6 days, associated with the Helmholtz-like resonance frequency. They concluded that this influence explained the discrepancy found by Garrett et al. (1985). They also claimed that the variation of wind over the Hudson Bay also has an influence, but discussed this in less depth. Webster and Narayanan (1988) applied a simple barotropic model, a streamfunction model with a rigid-lid, in an attempt to explain the observed current variability on the Labrador Shelf. They found that, in the period range of 2.8-5.5 days, volume transport through Hudson Strait, induced by both the variation of atmospheric pressure over Hudson Bay and the along-strait wind forcing over Hudson Strait, significantly contributes to the current variability on the northern part of the shelf. However, their model was less successful in the other period ranges they studied, namely 1.8-2.8 days and 5.5-11 days. For the longest period range (5.5-11 days), they argued that the failure might be caused by forcing not included in the model, e.g. the wind forcing within Hudson Bay, pressure forcing over the Canadian Arctic Archipelago, and wind forcing over Baffin Bay.

The sea level data used in these previous studies were collected from one coastal gauge at Nain, Labrador. From summer 1985 to summer 1987, bottom pressure data were collected at an array of pressure gauges on the Labrador and Newfoundland Shelf (Wright et al., 1988). The wide spatial distribution and sufficiently long time

duration of this dataset allow for a more thorough investigation to detect and examine the variability on the shelf. Middleton and Wright (1989) used a dynamical mode fitting technique to explain the bottom pressure variability on the Labrador Shelf in terms of the propagation of coastal trapped waves (CTWs), generated by the atmospheric pressure variation over Hudson Bay and remote wind forcing (to the north of the Shelf). In a later study (Middleton and Wright, 1991), they included the effect of local wind forcing, and the offshore influence through a "Kelvin wave" mode. An additional factor, the scattering of CTWs as they propagating over the rugged topography of the Shelf, was taken into account by Wright et al. (1991). They found that, from multiple regression analysis, the amplitude of CTW decreases much more rapidly along the shelf than it would on a smooth shelf, where it is dissipated by frictional stresses alone. They demonstrated the influence of the rugged topography using a numerical model under restricted boundary conditions. Another noticeable feature in their work is that the "offshore" influence on the bottom pressure variability is simply represented as the pressure near the shelf break – a crude approximation.

An investigation using this bottom pressure dataset and numerical modeling was carried out by de Young et al. (1992, hereinafter DGGV). They applied a model like that of GDGC except that it was driven using twice-daily ECMWF wind forcing. The model was solved in the frequency domain and investigated three discrete periods

(namely 4, 8 and 12 days) at synoptic time scales. The influence of remote forcing from the rest of the North Atlantic beyond the shelf, incorporated using the coarse North Atlantic model of GG driven by ECMWF wind forcing, was found to be important at the northern end of the shelf. Strong coherence between model and observation was obtained at the two shorter periods at sites near the coast and on the shelf, but the model underestimates the amplitude of variation in the observational data. Fitting a complex constant to their model results can dramatically improve the coherence, indicating some forcing mechanisms missed in their model. One obvious weakness in their work is that their attempt to study the influence from the Hudson Bay–Hudson Strait system was unsuccessful because of the difficulty of incorporating the Hudson Strait boundary condition. The rigid-lid approximation adopted in their model prevented the study of the non-isostatic response due to atmospheric pressure.

From the above summary of previous work, we find that in order to reproduce the bottom pressure signal of the observational data, a model capable of including atmospheric pressure forcing, the influence of the Hudson Bay–Hudson Strait system and the rest of the North Atlantic is needed. The success of the work of DGGV (and our results in the previous two chapters) encourages the use of ECMWF wind and atmospheric pressure as the forcing field to drive the model used in this thesis. Results from the four experiments listed in Table 2.1 and their comparison with observation

Table 5.1: Bottom pressure gauge information. Locations are shown in Fig. 5.1.

#	Station	Depth (m)	Latitude (°N)	Longitude (°W)	Start Date	Length (days)
1	Brownell	<5	59.42	63.85	12/ 8/85	357
2	Hebron	<5	58.18	62.62	12/ 8/85	357
3	Nain1	<5	56.55	61.68	11/ 8/85	357
4	Nain2	204	56.55	60.32	18/10/85	292
5	Nain3	175	56.95	59.26	17/10/85	292
6	Nain4	571	57.05	58.96	17/10/85	292
7	Hamilton1	109	53.63	55.74	7/ 7/85	390
8	Hamilton2	145	53.84	55.18	7/ 7/85	390
9	Hamilton3	200	53.73	53.61	6/ 7/85	390
10	Hamilton4	600	54.01	52.85	6/ 7/85	390
11	Grand1	183	47.40	51.80	23/ 4/86	372
12	Grand2	98	46.86	48.72	24/ 4/86	372

data are shown below.

5.2 Model Results

Bottom pressure data (Wright et al., 1988) at 12 sites are compared with model output of adjusted sea level (1 cm change in sea level corresponds to roughly 1 millibar variation in bottom pressure, as discussed in Chapter 2). Positions of the 12 gauges are listed in Table 5.1 and shown in Fig. 5.1. The 10 gauges located on the Labrador Shelf were deployed in the summer of 1985 for about one year. The remaining two gauges are chosen from another 17 gauges deployed in the summer of 1986 as representative

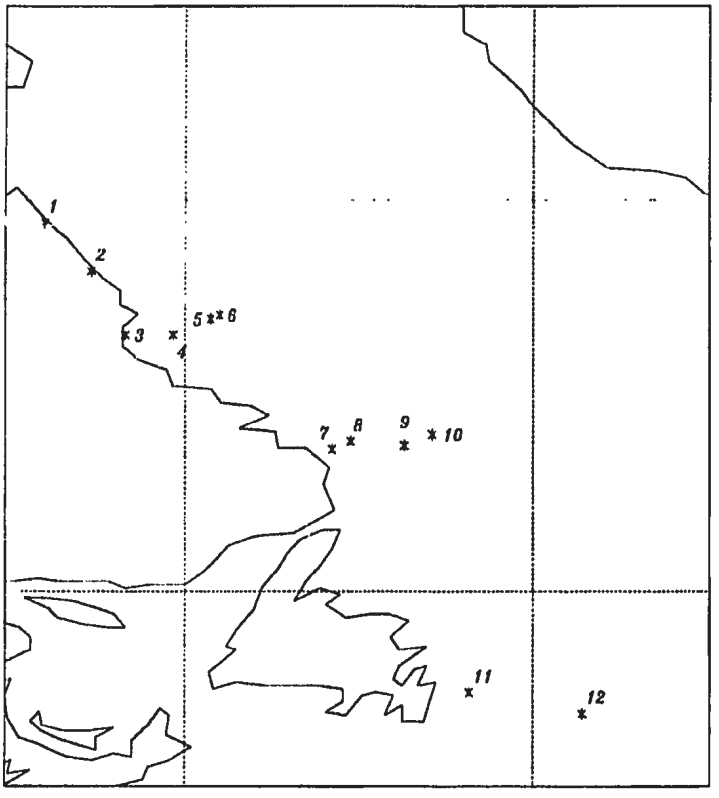

Figure 5.1: Locations of bottom pressure gauges as listed in Table 5.1

for the Grand Banks of Newfoundland. Note that only our primary model experiment (EXP1) extends to the latter half of the year 1986, when observed data at sites 11-12 are available. Tidal constituents in the observational data have been removed by harmonic analysis. A low-passed filter was then applied, which passed essentially all of the energy at periods beyond 2 days and less than 2% of the energy at periods less than 1 day. A low-passed filter with a cutoff period of 2 days is applied to the model output to remove the high frequency noise.

5.2.1 Time series

Time series of bottom pressure variation for 7 months in 1986 from both observation and EXP1, are presented in Fig. 5.2. The best agreement between model and observation is obtained at sites 11-12 on the Grand Banks, where the model reproduces even the detailed features in the observations. Good agreement is also found at sites located at the coast and the inner part of the shelf, although with detectable discrepancies. Toward the shelf break, the discrepancies increase, consistent with the result of DGGV.

To compare the behavior of different experiments, selected time series in the first two months of 1986 at five representative sites, namely sites 1,2,4,8 and 12, are plotted

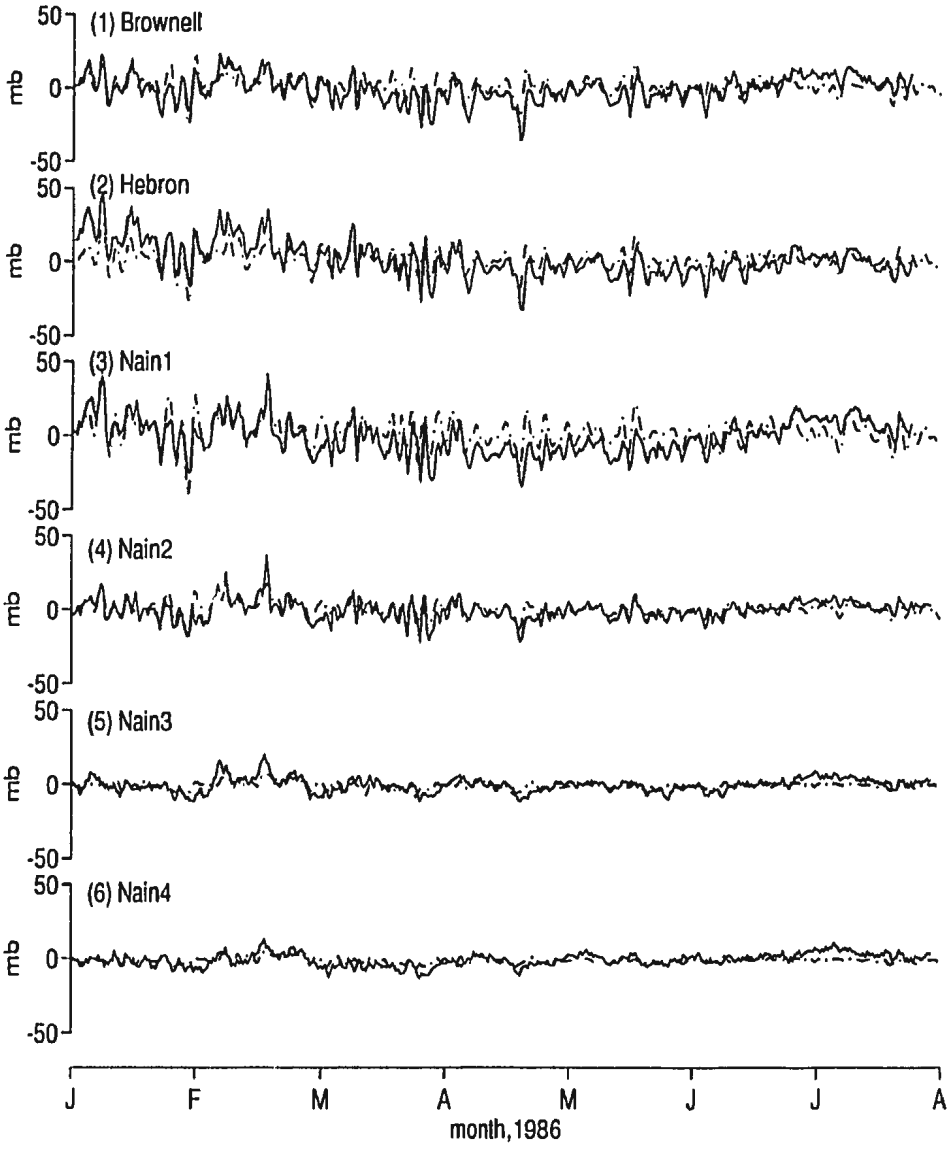

Figure 5.2: Time series for 7 months in 1986 of observed and modeled bottom pressure variation at 12 sites on the Labrador and Newfoundland Shelf. The time duration is from January 1 to 31 July for sites 1-10, from June 1 to December 31 for sites 11-12. Solid lines are from observation and dot-dashed lines are from EXP1. The number before the station name corresponds to the station number shown in Fig. 5.1.

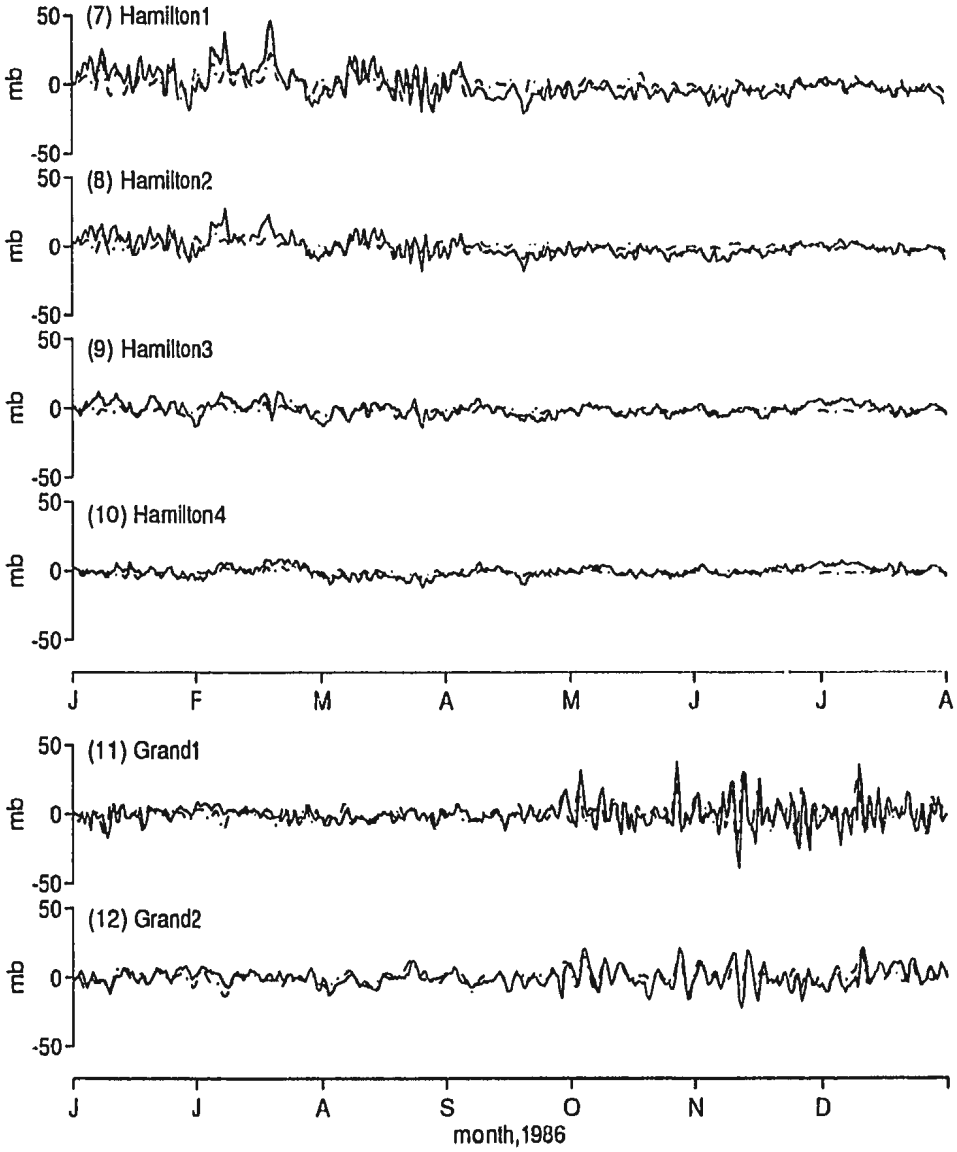

Figure 5.2: *(Continued)*

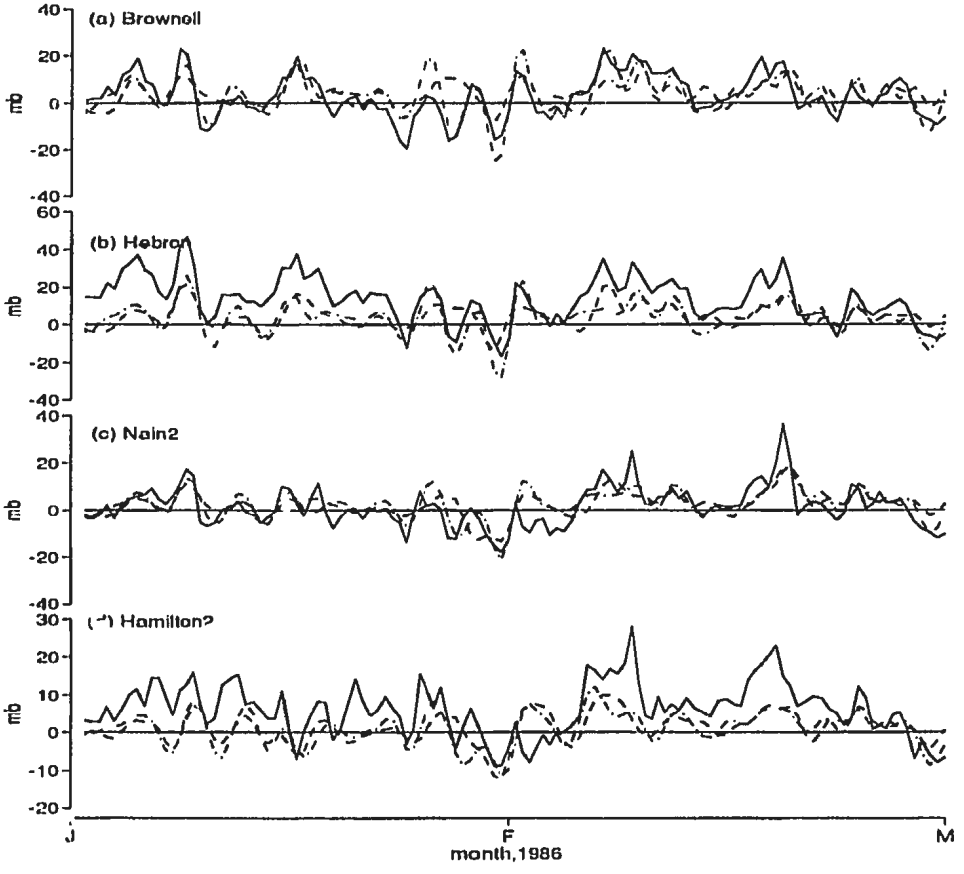

Figure 5.3: Selected time series at sites 1,2,4 and 8 for the first 2 months in 1986. Solid lines are from observation. Model results are for cases driven by both wind and atmospheric pressure forcings, with dot-dashed lines from EXP1 (Hudson Bay open) and dashed lines from EXP3 (Hudson Bay closed).

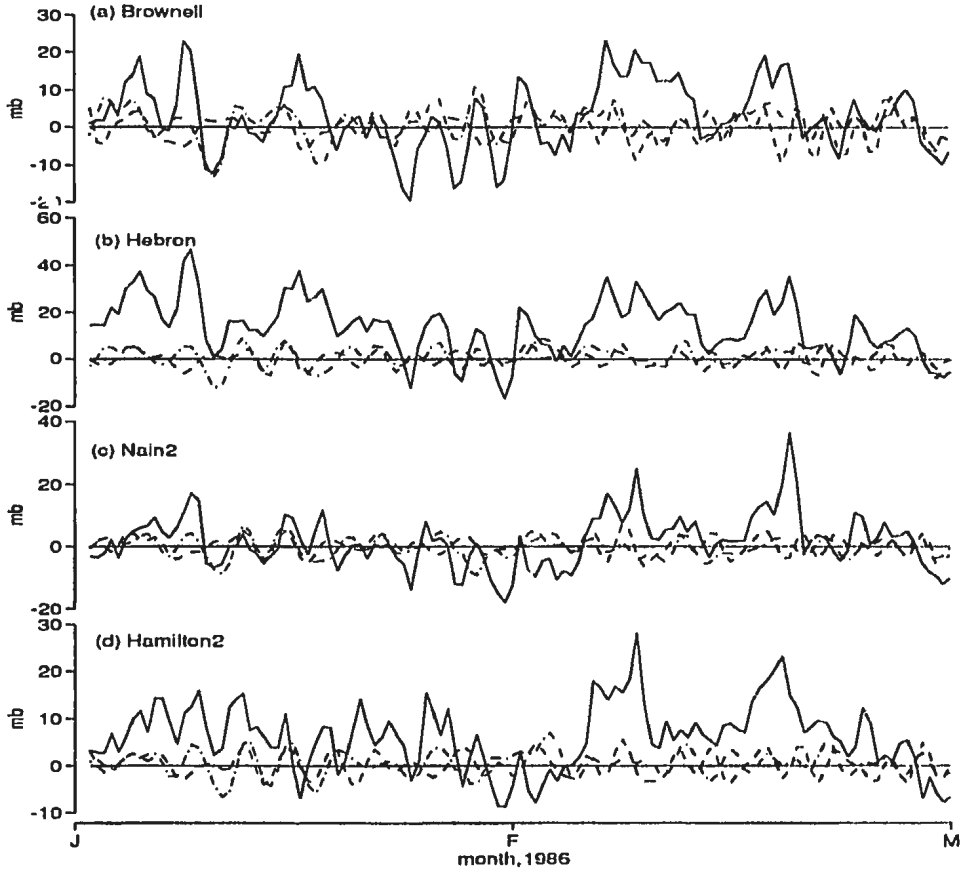

Figure 5.4: Same as Fig. 5.3 except that the model results are for cases driven by atmospheric pressure only. Dot-dashed lines are from EXP2 (Hudson Bay open) and dashed lines are from EXP4 (Hudson Bay closed).

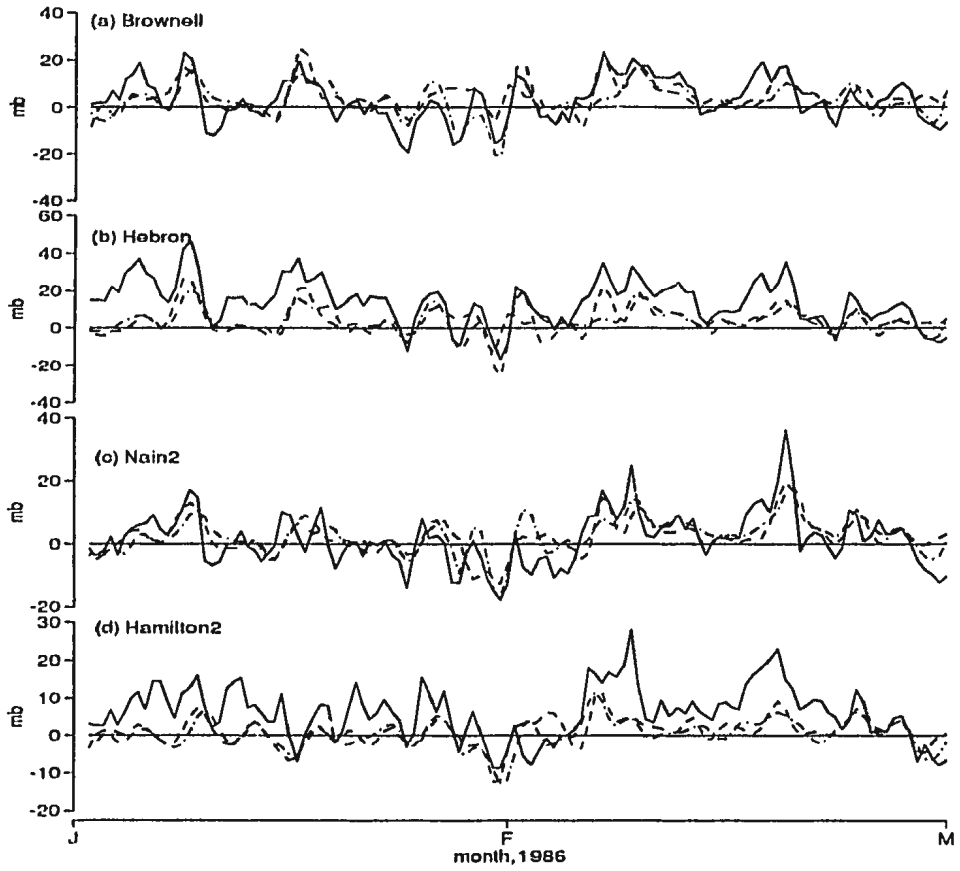

Figure 5.5: Same as Fig. 5.3 except that the model results are for "wind-only" driven cases. Dot-dashed lines are obtained by subtracting the results of EXP2 from EXP1 (Hudson Bay open) and dashed lines by subtracting EXP4 from EXP3 (Hudson Bay closed).

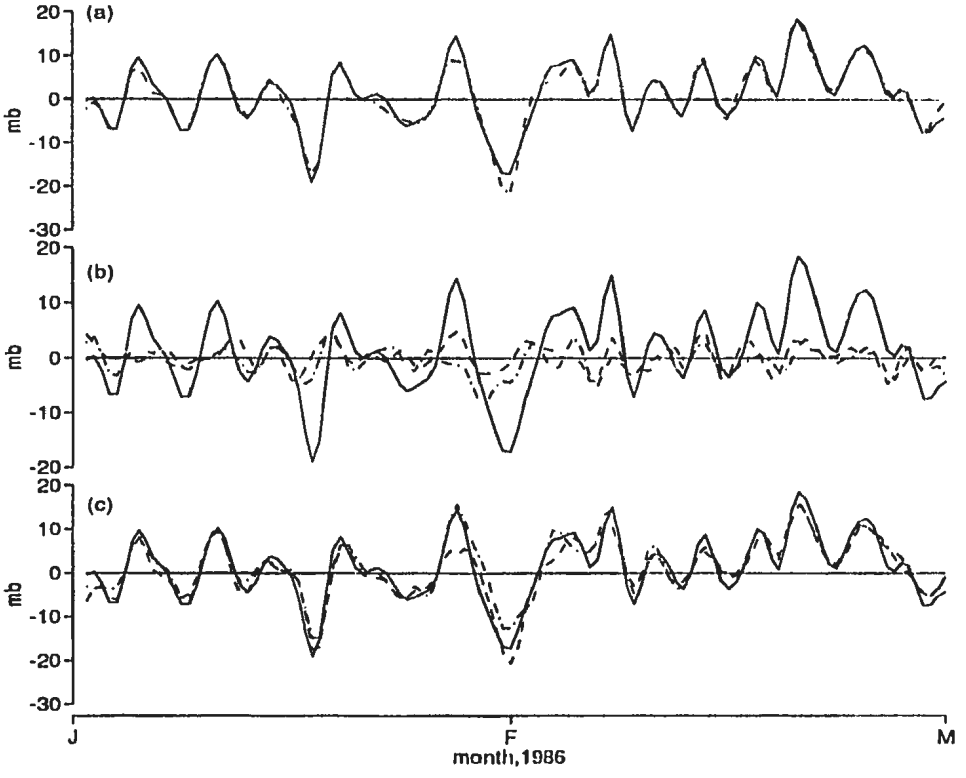

Figure 5.6: Selected time series for site 12 at Grand Banks for the first 2 months in 1986. Solid lines are from EXP1 and compared with, in (a), the dot-dashed line from EXP3 (wind and pressure driven cases); in (b), the dot-dashed line from EXP2 and dashed line from EXP4 (pressure-only driven cases); and in (c), the dot-dashed line obtained by subtracting the result of EXP2 from EXP1 and dashed line by subtracting EXP4 from EXP3 ("wind-only" driven cases). No observational data are available for this period.

in Figs.5.3-5.6. Fig. 5.3 and Fig. 5.6(a) compare the results of EXP 1 and EXP3, denoting the influence from the Hudson Bay–Hudson Strait system under both wind and atmospheric pressure forcings. The difference between the two is distinguishable for events at time scale of several days, at the four northern sites. Note one event at the end of January is captured by EXP1, but missed by EXP3. On the Grand Banks (site 12), the influence from the Bay/Strait system is barely detectable.

Figs. 5.4, 5.6(b) and Figs. 5.5, 5.6(c) show, respectively, the influence from the Bay/Strait system for the atmospheric pressure-only and "wind-only" driven cases. The results for the "wind-only" driven cases (Figs. 5.5 and 5.6(c)) are obtained by simply subtracting the results of atmospheric pressure-only driven cases from those under both forcings. These plots show that the atmospheric pressure-only driven cases are more influenced by the Bay/Strait system, the influence of this system being significant at all sites. The second point to note is that the contribution from wind forcing, with or without the Bay/Strait system, is more important than that from atmospheric pressure forcing. The results of statistical analysis stated below are intended to provide a better understanding of the behavior of different models at different time scales.

5.2.2 Statistical analysis

Results of coherence analysis are presented in Figs. 5.7-5.12. For the range of periods (beyond 2 days) resolved by the analysis, coherence significantly above the 95% confidence level and good phase fit between observation and EXP1, are obtained at sites 1, 2, 3, 4, 7, 8 and 12 (result at site 11 is quite similar with site 12). (Solid curves in Figs. 5.7(a)-(b), 5.8, 5.10 and 5.12(a)). The coherence peaks at synoptic time scales (~2-12 days) are obvious at these sites.

Across Nain Bank (Fig. 5.8) and Hamilton Bank (Fig. 5.10), coherence level decreases significantly from the coast to the shelf break. Coherence peaks at synoptic time scales are still detectable at sites 5,6,9 and 10, but some are only marginally above the 95% confidence level.

With the Hudson Bay–Hudson Strait system included, models driven by atmospheric pressure only (EXP2) and "wind-only" (EXP1 with EXP2 subtracted) still generate coherence peaks on the Labrador Shelf, as illustrated by the dashed and dot-dashed curves in Figs. 5.7(a)-(b), 5.8 and 5.10. Coherence between observation and EXP2, the atmospheric pressure-only driven case, decreases down (southward) the shelf, whereas the influence from wind forcing increases. The contribution from atmospheric pressure forcing is important from the north end of the shelf to Nain

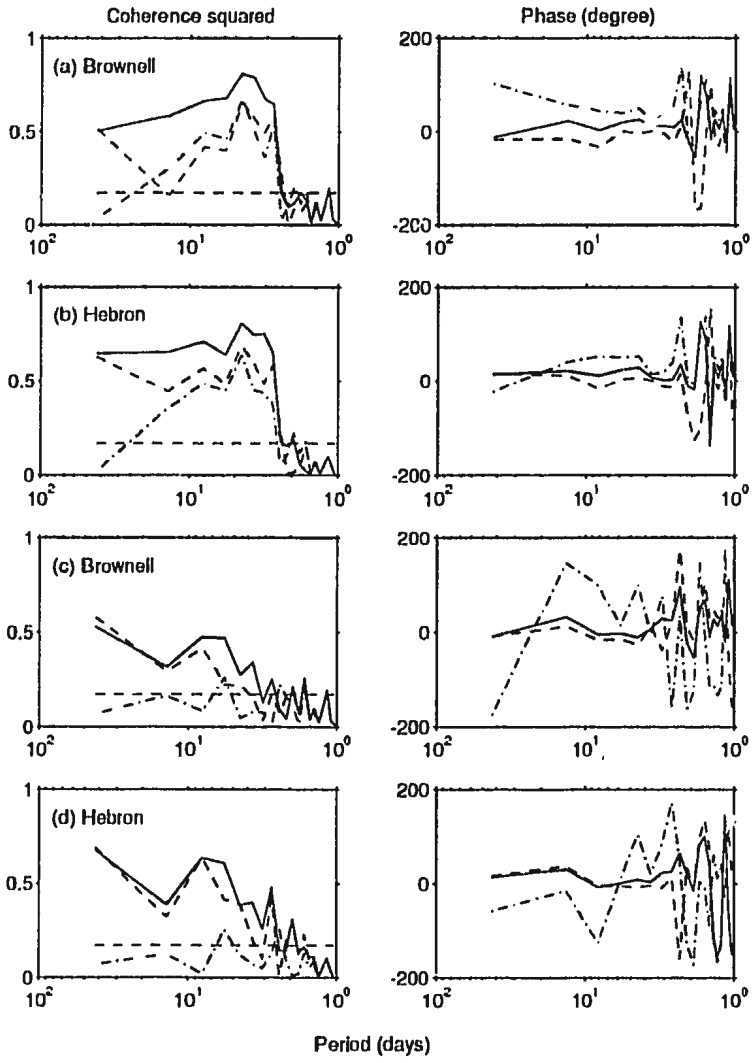

Figure 5.7: Coherence squared and phase lag between observed and modeled bottom pressure variation at sites 1-2. In (a) and (b), the models are for Hudson Bay open cases. The solid curves are observation (OB) vs. EXP1; dot-dashed curves OB vs. EXP2; and dashed curves are OB vs. EXP1 with EXP2 subtracted. In (c) and (d), the models are for Hudson bay closed cases. The solid curves are OB vs. EXP3; dot-dashed curves OB vs. EXP4; and dashed curves are OB vs. EXP3 with EXP4 subtracted. Coherence above the horizontal dashed lines is significant at the 95% level. Positive phase means observation leads model.

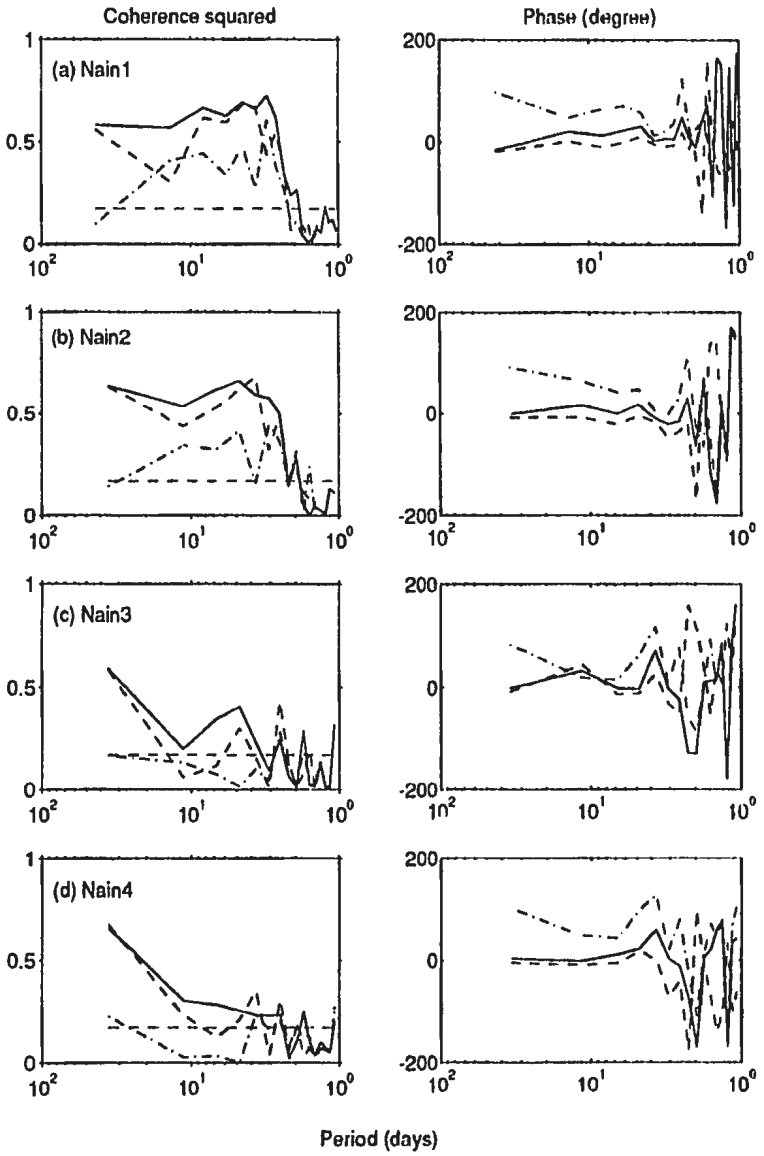

Figure 5.8: Same as Fig. 5.7(a) and (b) for the Hudson Bay open cases but at sites 3-6 across Nain Bank. solid lines are OB vs. EXP1; dot-dashed curves OB vs. EXP2; and dashed curves are OB vs. EXP1 with EXP2 subtracted.

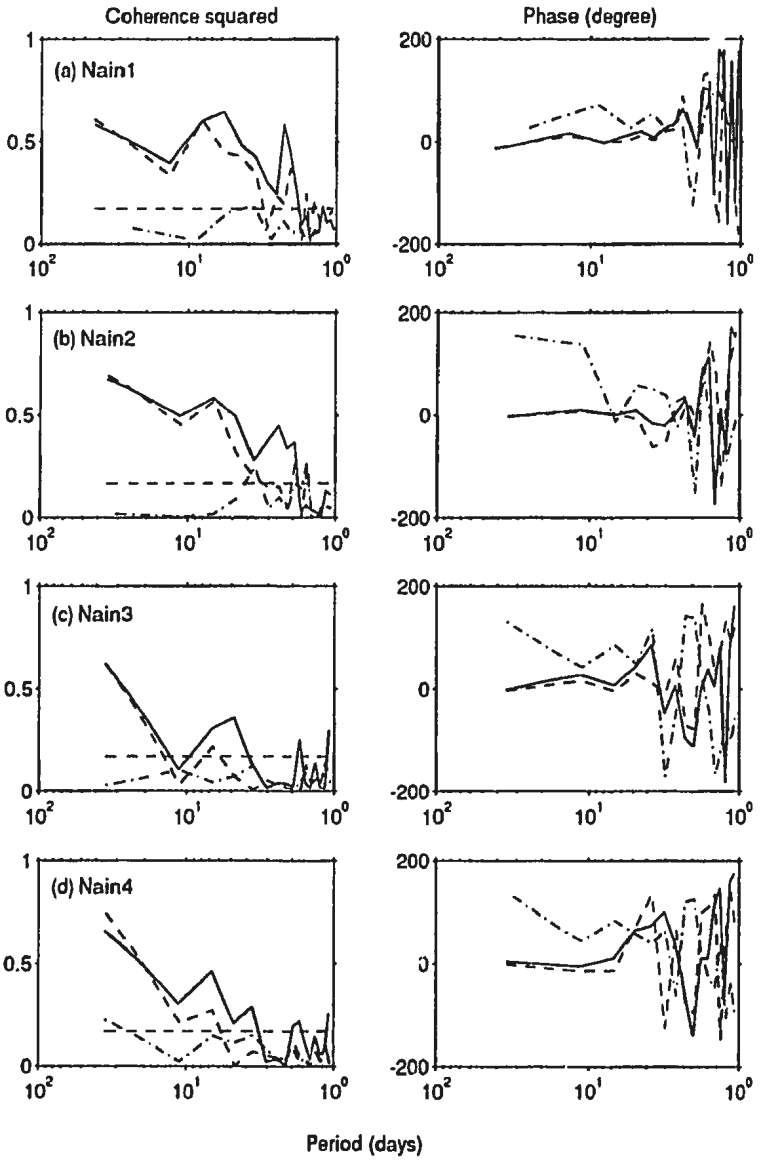

Figure 5.9: Same as Fig. 5.7(c) and (d) for Hudson Bay closed cases but at sites 3-6 across Nain Bank. solid curves are OB vs. EXP3; dot-dashed curves OB vs. EXP4; and dashed curves are OB vs. EXP3 with EXP4 subtracted.

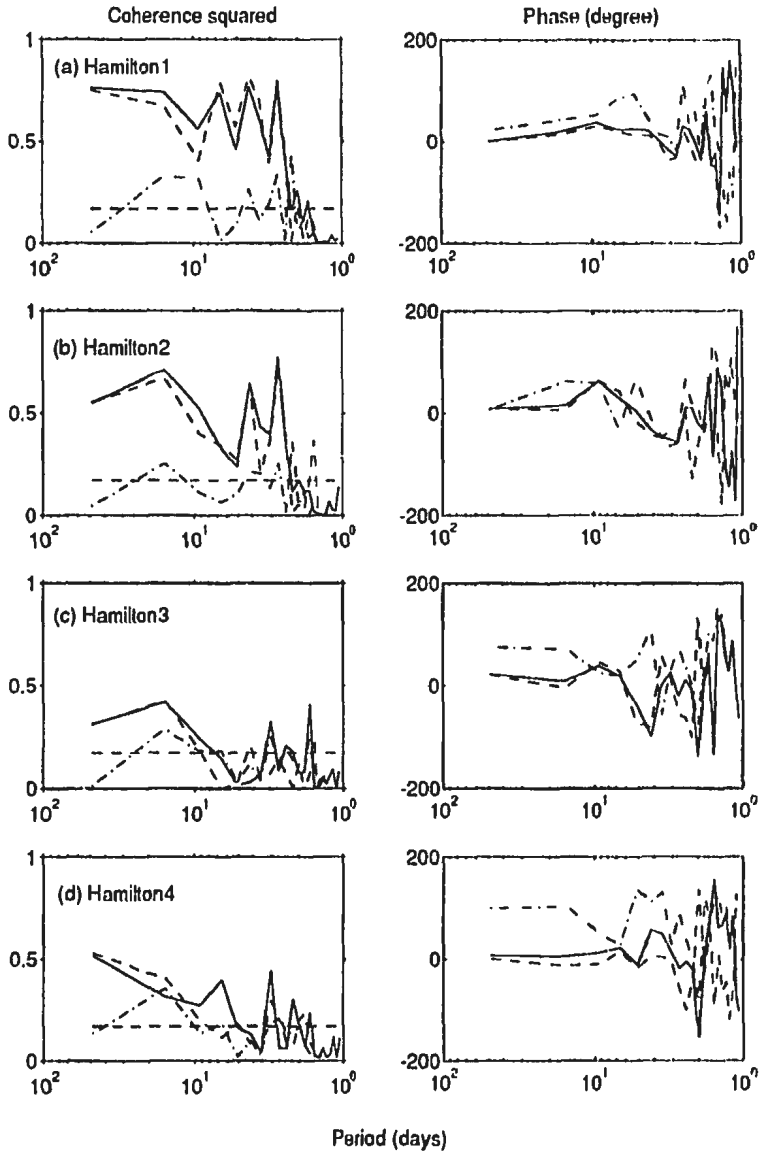

Figure 5.10: Same as Fig. 5.8 but at sites 7-10 across Hamilton Bank.

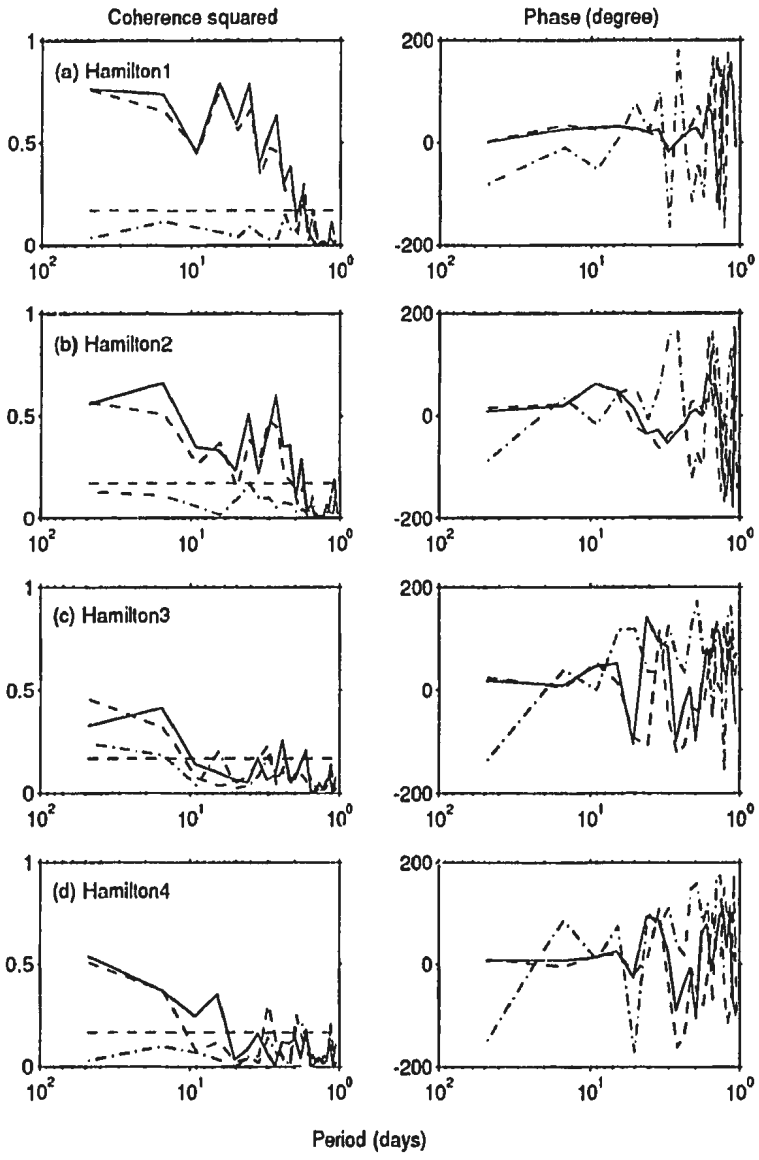

Figure 5.11: Same as Fig. 5.9 but at sites 7-10 across Hamilton Bank.

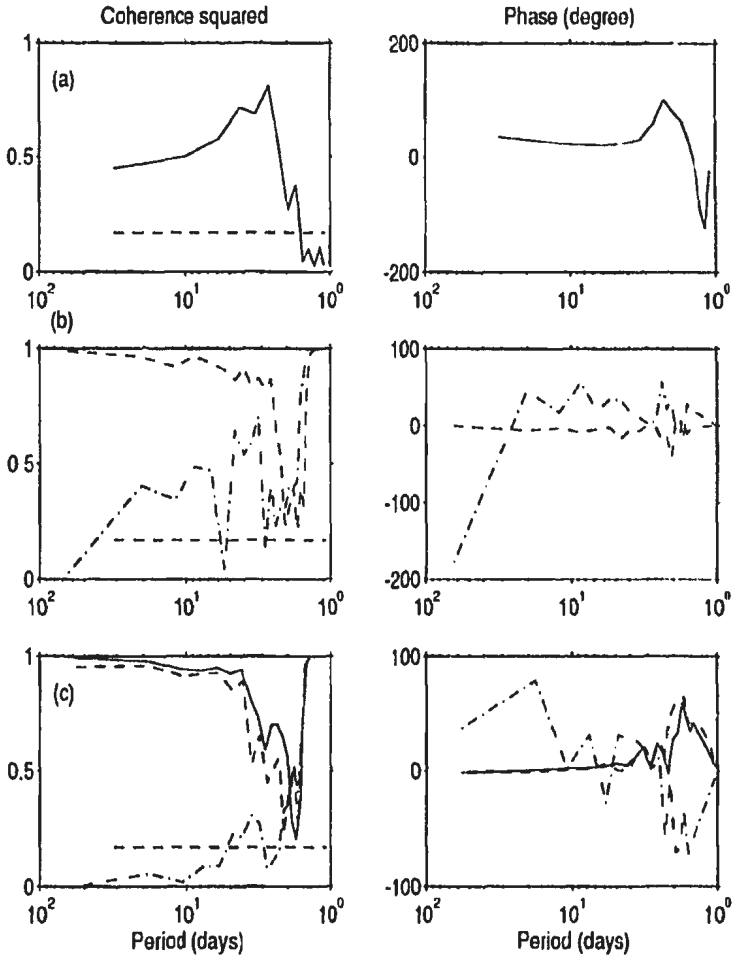

Figure 5.12: Coherence squared and phase lag, at site 12 on the Grand Banks, of (a) OB vs. EXP1; (b) EXP1 vs. EXP2 (dot-dashed curves) and EXP1 vs. EXP1 with EXP2 subtracted (dashed curves); and (c) EXP1 vs. EXP3 (solid curves), EXP1 vs. EXP4 (dot-dashed curves) and EXP1 vs. EXP3 with EXP4 subtracted (dashed curves). Coherence above the horizontal dashed lines is significant at the 95% level. Positive phase means the first leads the second in a pair.

Bank, but not on Hamilton Bank and the Grand Banks (Fig. 5.12(a)). Wind forcing is important at all the periods resolved.

Closing the Bay/Strait system, coherence peaks at synoptic time scales decreases dramatically, especially at periods of $\sim$ 3-5 days (as shown in Figs. 5.7(c) (d), 5.9 and 5.11). Although coherence peaks at synoptic time scales still exist at most sites, they are generated by wind forcing only and located at periods of $\sim$6-10 days, particularly at and to the north of Nain Bank. No coherence peaks are generated by atmospheric pressure forcing only when the Bay/Strait system is closed.

On the Grand Banks (site 12), as no observational data are available for the period when EXP2, EXP3 and EXP4 are run, only coherence between EXP1 and these experiments is calculated. The results (Fig. 5.12(b) and (c)) show that at periods beyond $\sim$3 days, coherence between EXP1 and EXP3, the two wind and pressure driven cases, and between EXP1 and the "wind-only" driven cases are high and the influence of the Bay/Strait system is weak. The influence of the Bay/Strait system for the atmospheric pressure-only driven cases is detectable at site 12.

The ability of the models to reproduce the energy distribution in the observed bottom pressure variation and the contribution from individual forcing and the influence of Hudson Bay--Hudson Strait system are demonstrated in the variance conserving spectra plots in Figs. 5.13-5.16. At the north end of the shelf, sites 1-2, and

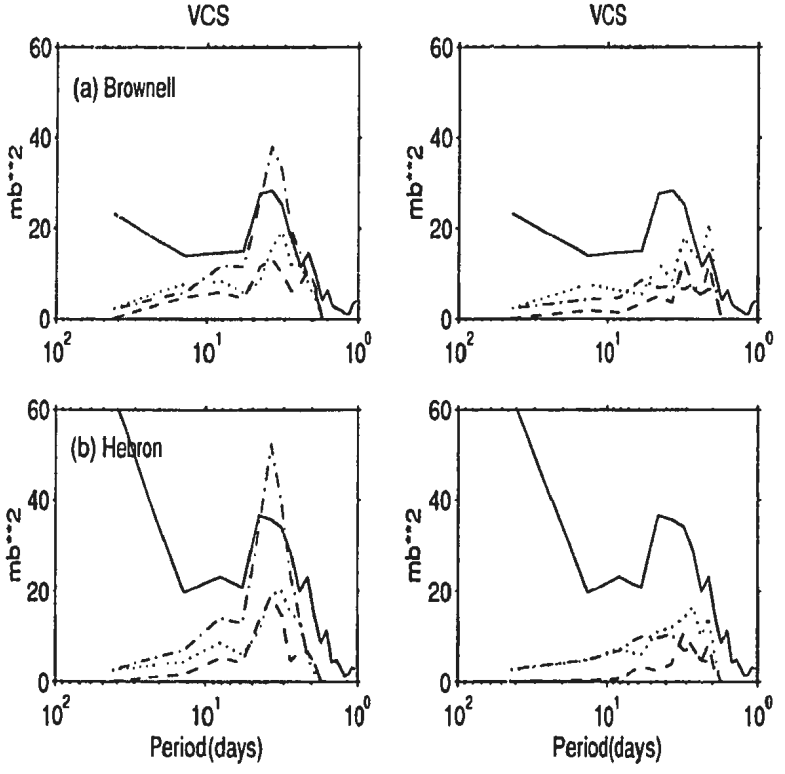

Figure 5.13: Variance conserving spectra of observed and modeled bottom pressure variation at sites 1-2. The solid curves are from observation. Model results in the left panels are for the Hudson Bay open cases, with dot-dashed curves from EXP1, dashed lines from EXP2, and dotted curves from EXP1 with EXP2 subtracted; Model results in the right panels are for the Hudson Bay closed cases, with dot-dashed curves from EXP3, dashed lines from EXP4, and dotted curves from EXP3 with EXP4 subtracted.

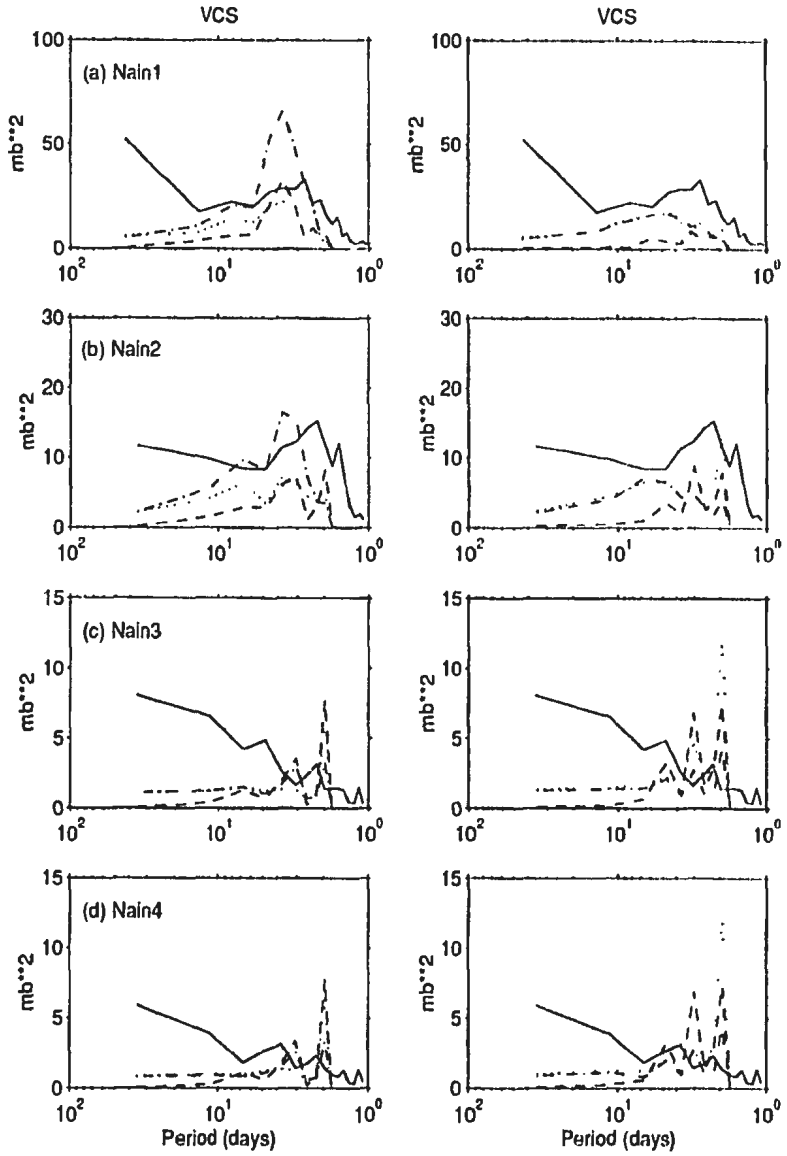

Figure 5.14: Same as Fig.5.13 but for sites 3-6 across Nain Bank.

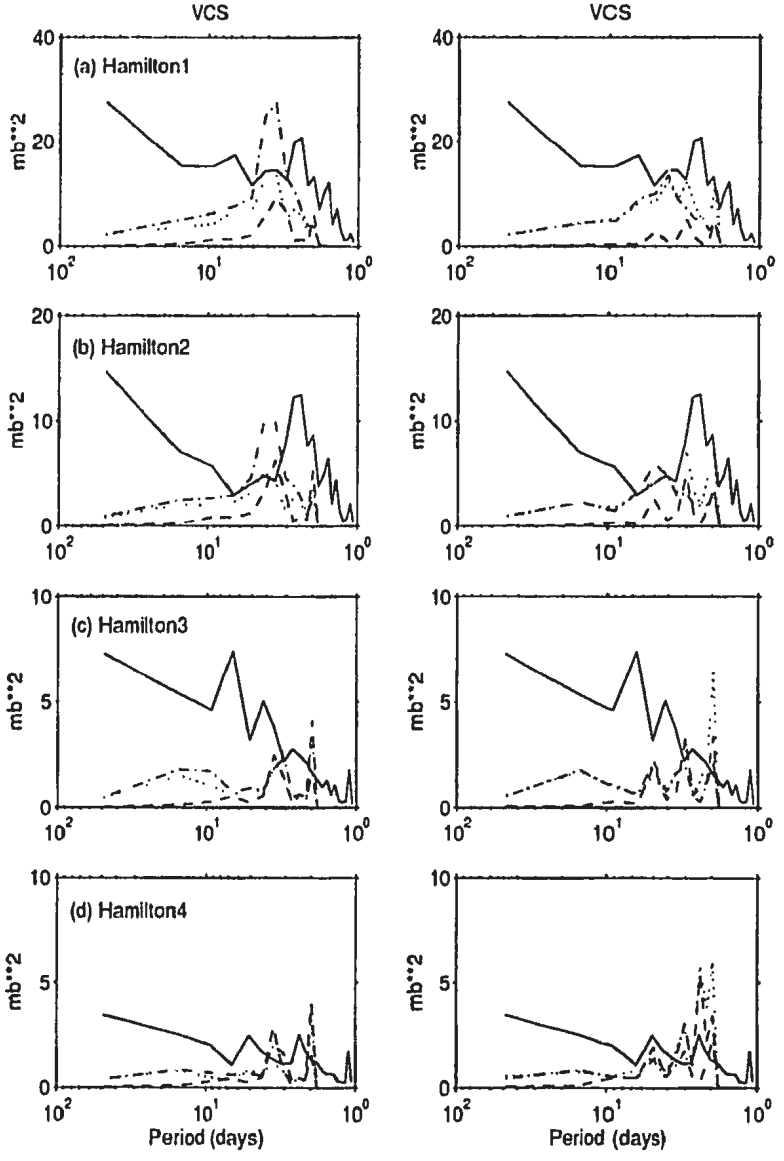

Figure 5.15: Same as Fig.5.13 but for sites 7-10 across Hamilton Bank.

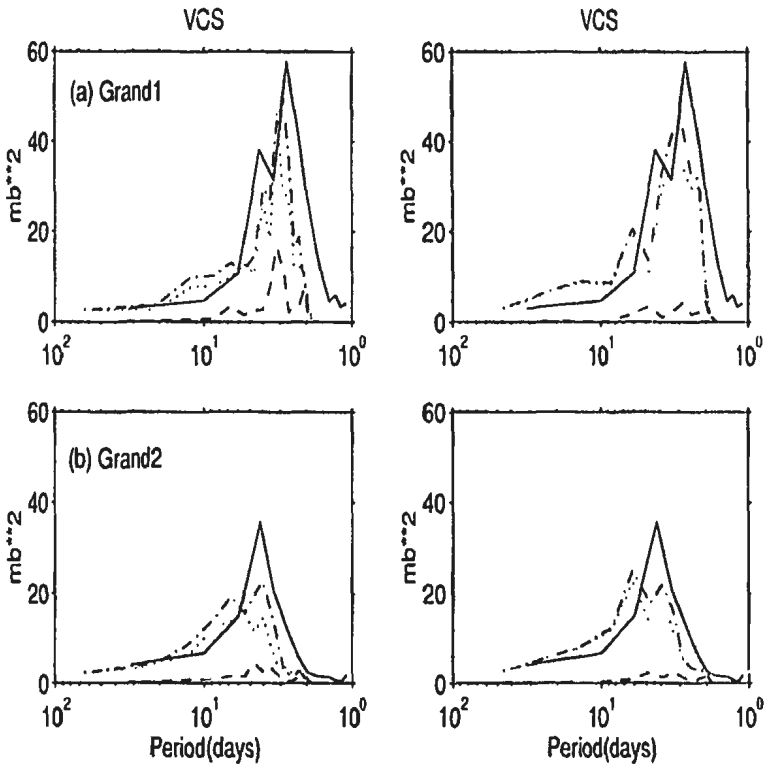

Figure 5.16: Same as Fig.5.13 but for sites 11-12 on the Grand Banks.

on the Grand Banks, sites 11-12, EXP1 explains quite well the energy distribution at synoptic time scales of ~2-12 days. An energy peak at periods of ~2-6 days is generated at all sites by EXP1, being fairly coincident with observation at sites 1-2 and 11-12. The model overestimates the energy peak at site 3, the coastal gauge at Nain. Peaks in the observational data at the inner site of Nain Bank and Hamilton Bank (sites 4, 7 and 8) tend to shift to a higher frequency band (corresponding to periods of 2-3.5 days). This tendency, however, is not captured by the model. Another feature to be noticed is that the observations exhibit an increase in energy with decreasing frequency at periods beyond synoptic time scales, at all sites except at sites 11-12 on the Grand Banks. This feature, however, is not captured by the model.

The significant contribution from atmospheric pressure forcing only with the Bay/Strait system included (results of EXP2), is to generate the energy peaks at periods of ~2-6 days. The "wind-only" driven cases also generates peaks at this period range. Contributions from the two at periods of ~2-6 days are comparable on the Labrador Shelf, but the effect of wind dominates that of atmospheric pressure at other periods and at all the periods on the Grand Banks.

For cases driven by both wind and atmospheric pressure forcings, closing the Bay/Strait system causes a significant reduction in energy density at ~2-6 days period, at and to the north of Hamilton Bank. The energy peak induced by atmospheric

pressure only, as found in the Hudson Bay open case, now disappears totally. Closing the Bay/Strait system also causes changes in energy induced by "wind-only" at this period range, especially at the northern end of the Shelf. The influence of the Bay/Strait system on the Grand Banks is unimportant.

5.2.3 Contour maps

Contour maps of adjusted sea level (corresponding to bottom pressure) from EXP1 at four continuous days at the end of January 1986 are given in Fig. 5.17. Variations of bottom pressure on the Labrador Shelf, in the form of coastal trapped wave (CTW) propagation, are evident. Significant changes within the Hudson Bay Hudson Strait system, generated by both wind and atmospheric pressure forcings, can be noticed. These changes propagate along Hudson Strait, which connects Hudson Bay to the outer ocean, and influence sea level (bottom pressure) on the Labrador Shelf. Driven by atmospheric pressure only (Fig. 5.18 from EXP2), both the changes within the Bay and on the Shelf diminish significantly, indicating the important role played by wind forcing. Changes within Hudson Bay, caused by atmospheric pressure forcing only, still have an influence on the Labrador Shelf. Closing the Bay/Strait system, but maintaining both forcing terms (Fig. 5.19 from EXP3), the contour pattern is

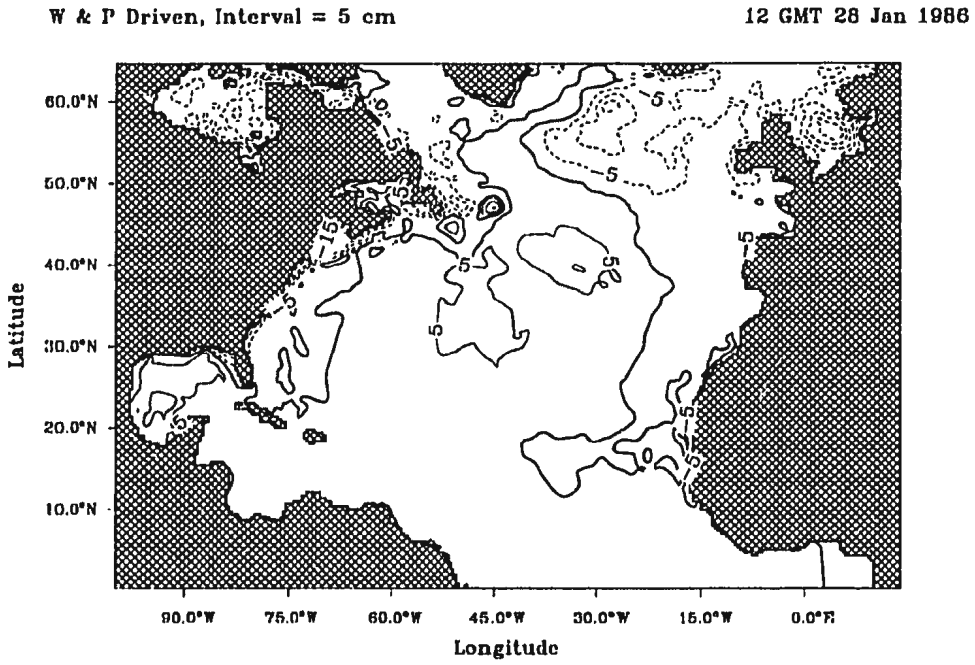

Figure 5.17: Contours of adjusted sea level obtained from EXP1 at 12 GMT, 28-31 January 1986. The contour interval is 5 cm. Thinner solid lines are positive and dashed lines are negative. The thick solid lines are zero.

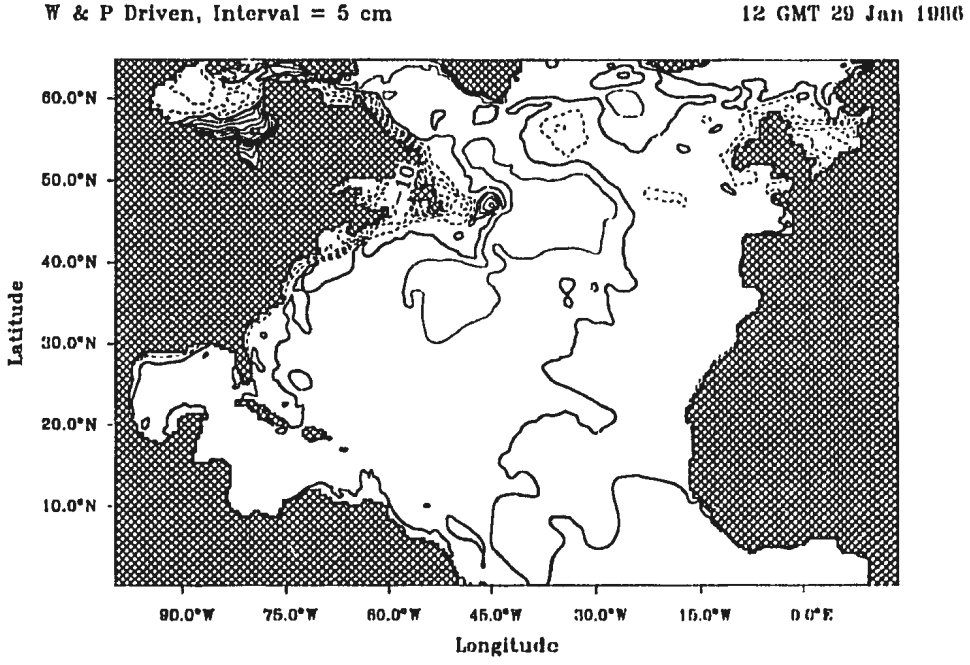

Figure 5.17: (*Continued*)

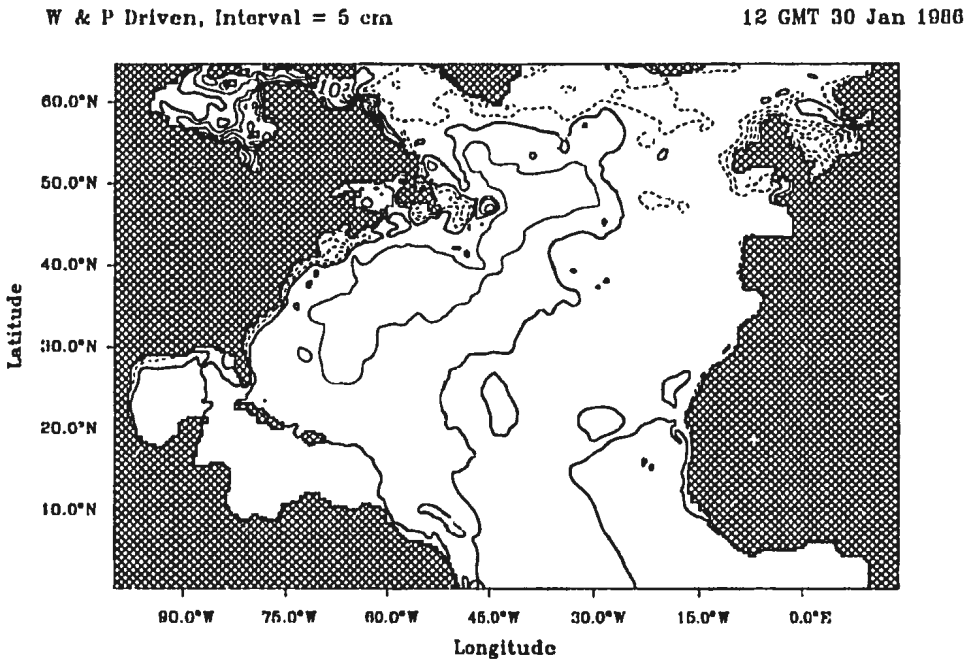

Figure 5.17: (*Continued*)

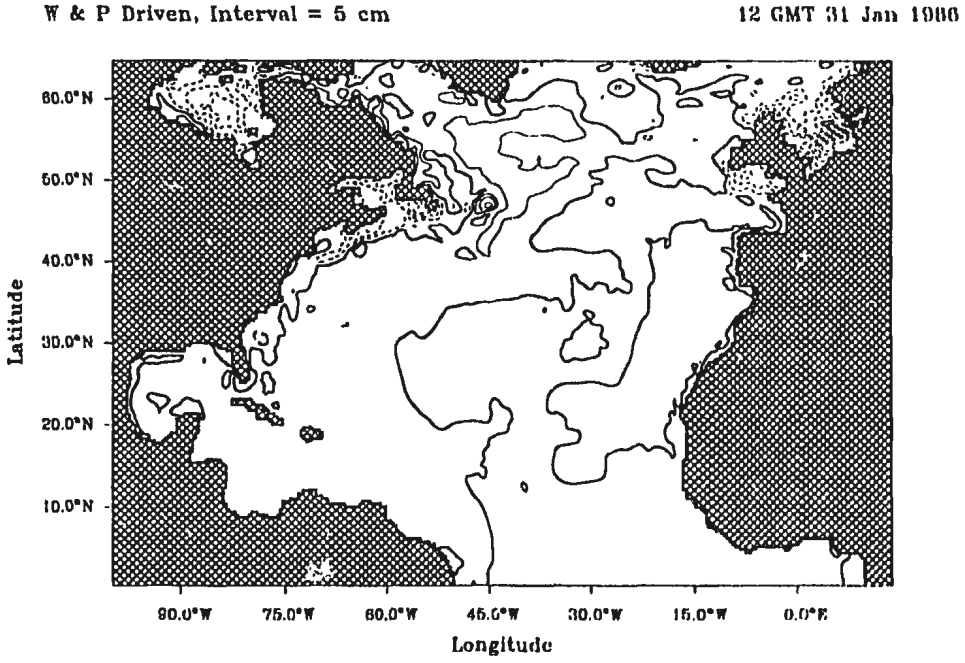

Figure 5.17: (*Continued*)

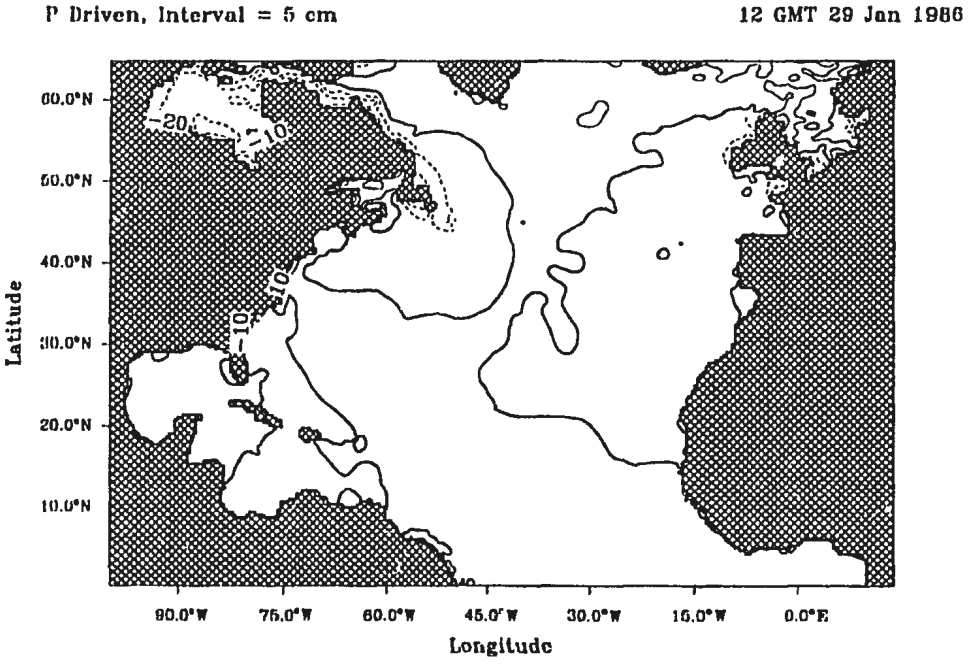

Figure 5.18: Same as Fig. 5.17 but from EXP2, at 12 GMT, 29-30 January 1986.

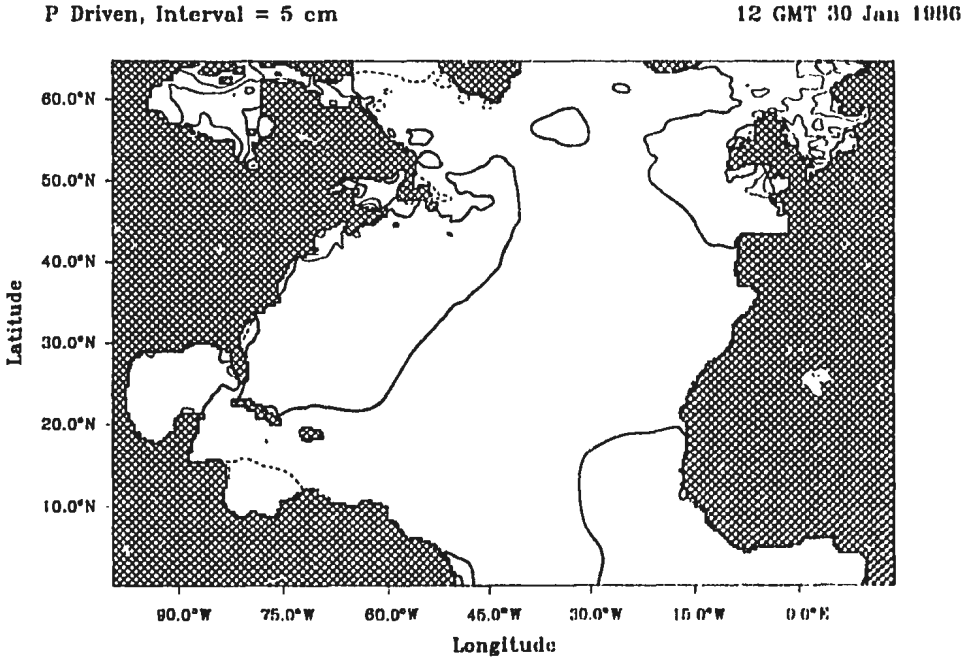

Figure 5.18: (*Continued*)

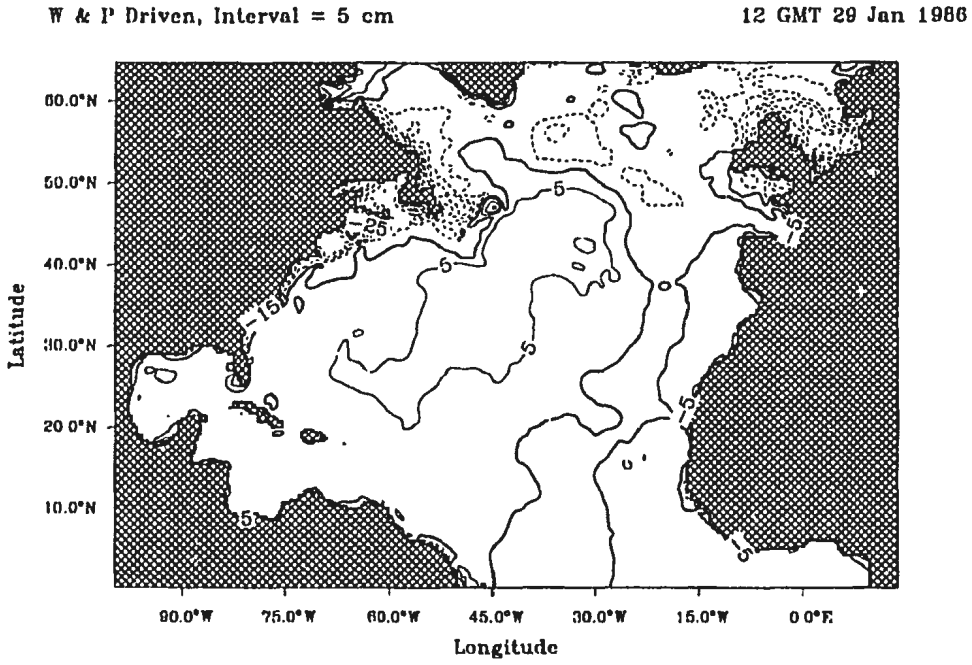

Figure 5.19: Same as Fig. 5.18 but from EXP3.

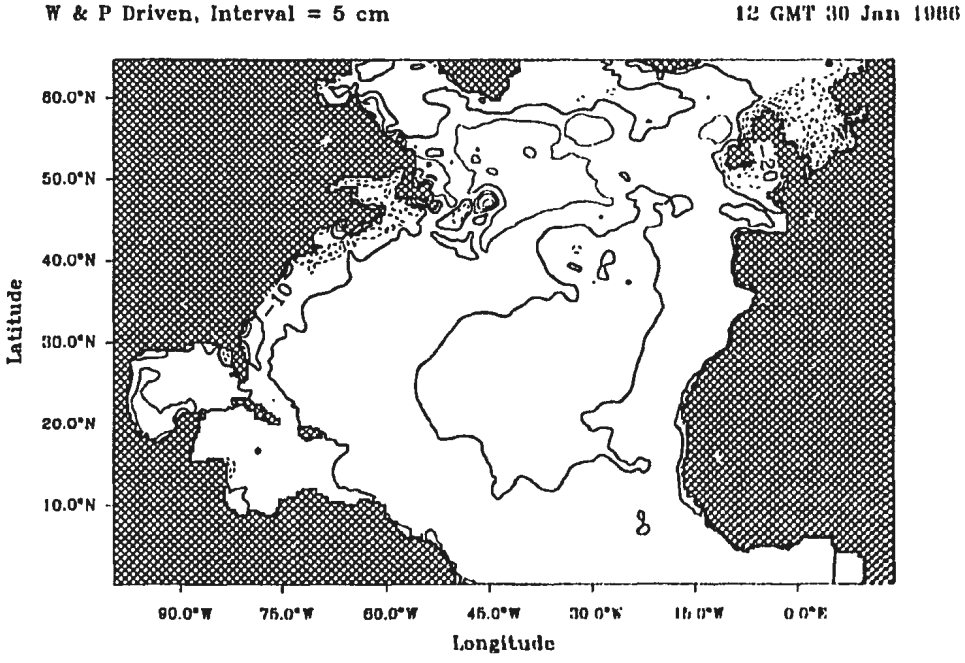

Figure 5.19: (*Continued*)

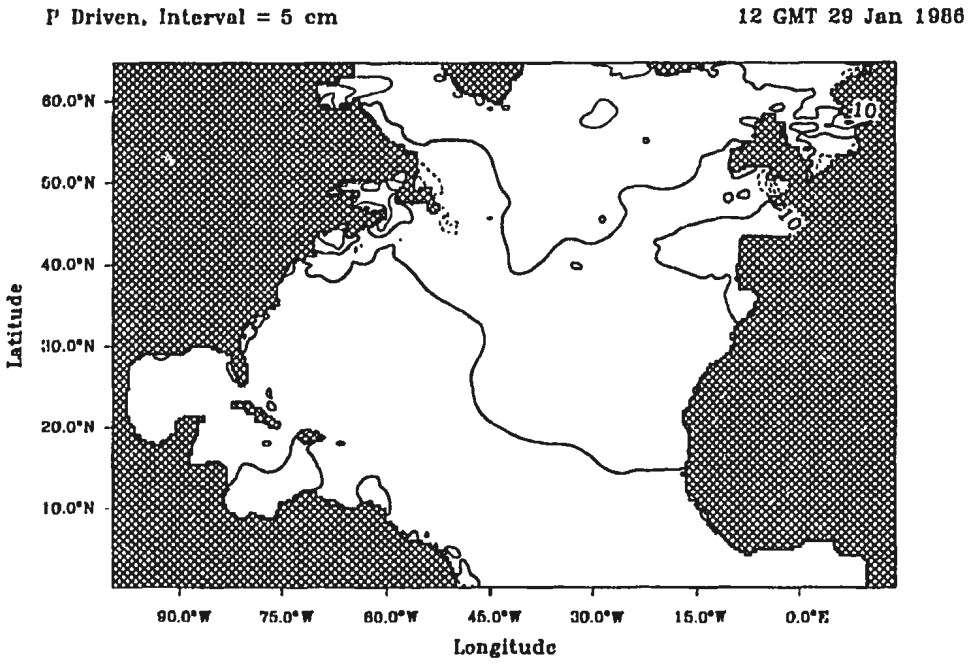

Figure 5.20: Same as Fig. 5.18 but from EXP4.

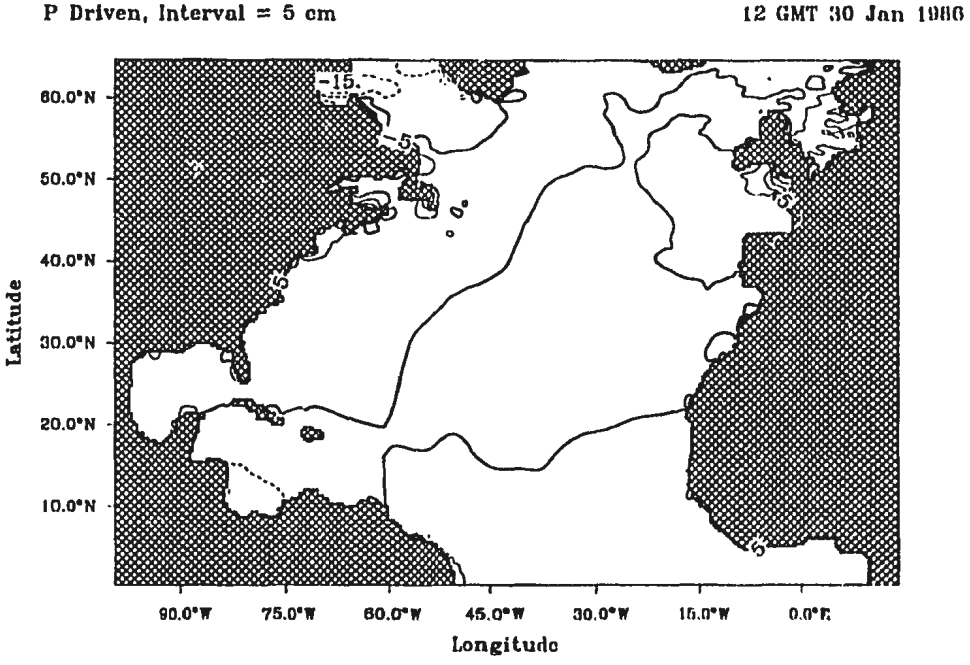

Figure 5.20: (*Continued*)

similar to that obtained from EXP1, but significant differences can be observed on the Labrador Shelf (compare maps of January 30 in Figs. 5.17 and 5.19). Without the Bay/Strait system, atmospheric pressure forcing itself (Fig. 5.20 from EXP4) can account for almost none of the variation (compare maps of January 29 in Figs. 5.20 and 5.18). This indicates that the important contribution of atmospheric pressure forcing comes from the Bay/Strait system.

5.3 Discussion

The above results show that EXP1 can explain the observed bottom pressure variation on the Labrador and Newfoundland Shelf, at synoptic time scales of ~2-12 days . Coherence at longer time scales is also quite significant, although the model does not capture the tendency of increasing energy with decreasing frequency on the Labrador Shelf. The success of the barotropic model indicates the relatively unimportant role played by stratification in the bottom pressure variability at synoptic time scales. In fact, Middleton and Wright (1989) estimated the buoyancy frequency N to be 2-3 cph at 100 m and decreasing to 0.5 cph at a depth of 400 m or greater. Comparing with the values for the Eastern Australian Shelf, $N \simeq 5.7$ cph at 100 m and $N \simeq 2.9$ cph at depth of 400 m (Church et al., 1986), one can draw a conclusion that the Labrador

Shelf is weakly stratified.

Numerical experiments successfully reveal the influence from the Hudson Bay Hudson Strait system on the Labrador Shelf, a hypothesis proposed by Wright et al. (1987) and later extended by Webster and Narayanan (1988). It is confirmed that under atmospheric pressure variation, the Bay/Strait system does generate a significant non-isostatic response on the Labrador Shelf at synoptic time scales, with energy peaks centered at 2-6 days, corresponding to the Helmholtz-like resonance frequency (~3.4 days) as deduced by Wright et al. (1987). Closing the Bay/Strait system, the energy peak induced by atmospheric pressure disappears.

Comparing the result of the atmospheric pressure-only driven case with that of the "wind-only" driven cases, we find that wind forcing is more important than atmospheric pressure forcing. Energy peaks at periods of 2-6 days also drop by closing the Bay/Strait system, indicating that winds over the Hudson Bay Hudson Strait must be included to explain the unusual non-isostatic response on the Labrador Shelf first reported by Garrett et al. (1985). The model driven by both forcings gives better agreement with observations than driven by individual forcing.

The relevance of coastal trapped waves (CTW) propagation in explaining the variability on the Labrador Shelf has been discussed by Middleton and Wright (1991). Our finding that the influence from the Bay/Strait system decreases down the Shelf

indicates the scattering of CTWs by the rugged topography of the Shelf. Our primary experiment, EXP1, gives the best agreement with observation at the north end of the Shelf, being the origin of CTWs; and on the Grand Banks, where the CTWs are expected to have been dissipated through scattering as they propagate over the rugged topography of the Labrador Shelf. However, weaker agreement is obtained in between, i.e., on the Nain Bank and Hamilton Bank, and especially at the offshore sites. It may be that the topography data used in the model experiments does not properly represent the real topography of the Shelf and slope. A topography with higher resolution, more representative of the rugged nature of the Shelf, should be adopted to examine this effect. Another possible reason may be the exclusion of stratification in the barotropic model. Stratification may be important in affecting the propagation of shelf waves, particularly in the presence of strongly varied topographic features. However, DGGV did an experiment by incorporating the effect of stratification through a JEBAR (the Joint Effect of Baroclinity And Topographic Relief) term, which did not exhibit significant difference from their purely barotropic case.

Toward the shelf break, the model shows poor agreement with observation, a result consistent with that of DGGV. The imperfect formulation of topography and the exclusion of stratification may still cause the discrepancy. Other factors may also

be responsible. One candidate is mesoscale eddies on the Labrador Shelf. Mesoscale ice-edge meanders off the Labrador coast have been observed in satellite imagery (LeBlond, 1982; Ikeda, 1987) and might be expected to play important roles at the shelf break.

Finally, regions not included in our model domain, such as Baffin Bay and the Canadian Arctic Archipelago, as claimed by Webster and Narayanan (1988), may also have influence on the Labrador Shelf, particularly at longer time scales. One interesting extension of this work would be to include Baffin Bay in the model domain.

Chapter 6

Summary and Conclusions

The barotropic response of the North Atlantic to wind and atmospheric pressure forcing is studied with a two-dimensional, fine-resolution barotropic model. The model domain extends from the equator to 65°N and from 100 °W to 14°E with a resolution of 1/3° in latitude and 2/5° in longitude. The forcing field used to drive the model is the twice-daily wind and atmospheric pressure data from the European Center for Medium Range Weather Forecasts (ECMWF). The agreement obtained between model results and observational data suggests that the ECMWF data provide realistic forcing fields.

The primary model experiment, EXP1, is a two-year (1985-1986) run driven by both wind and atmospheric pressure forcings. Three one-year runs are designed to

determine the contribution from individual forcing and the influence from the Hudson Bay–Hudson Strait system. They are, respectively, EXP2, atmospheric pressure-only driven, applied to the whole domain as in EXP1; EXP3, driven by both forcings, and EXP4, by atmospheric pressure only, applied to a domain with the Hudson Bay–Hudson Strait system excluded. The response to "wind only" forcing is derived by simply subtracting the results of EXP2 from EXP1 or EXP4 from EXP3, as our parameter tests show that nonlinearities introduced by our choice of quadratic bottom friction are not important.

The time scales being studied range from several days to seasonal. Compared with the sea level data observed at tide gauges along the coast, EXP1 gives best agreement with observation at locations with a broad shelf, where the stratification effect is expected to be weak. Significant coherence between observed and model-calculated adjusted sea level is obtained at periods beyond ~3 days, at four representative stations along the western boundary. A drop in coherence at ~12 days is found at Fernandina Beach, Florida, which may be due to the exclusion of advection by the mean flow in linear barotropic models. The steric effect not removed from the observational data is one reason for the discrepancies at longer time scales. The contribution of atmospheric pressure in inducing the non-isostatic sea level response is negligible at periods beyond ~2-3 days, but not in special regions as on Labrador

Shelf.

Compared with the cable data of Larsen (1992), EXP1 well explains the volume transport variation through the Florida Straits at synoptic time scales (~3-8 days). This result is consistent with that of Lee and Williams (1988) from a simple channel model forced by local winds, indicating that the local wind forcing is important at synoptic time scales. Significant coherence between observation and model is obtained at periods up to 50 days. A drop of coherence at ~10 days is found, suggesting, once again, a possible role for advection by the mean flow, not included in the present model. The model does quite well in capturing the variation at longer time scales in 1985, but not in 1986. As the cable data exhibit strong year to year variations taking place during this period, this provides an interesting question for further study.

Model experiments explain the variability in the bottom pressure data from the Labrador and Newfoundland Shelf. The significant non-isostatic response in the observational data at synoptic time scales (~2-12 days) is reproduced by model experiments with the Hudson Bay–Hudson Strait system included, with energy peaks at ~2-6 days. The contribution from atmospheric pressure forcing is only important in generating the energy peak at ~2-6 days when the Bay/Strait system is included. This verifies the hypothesis proposed by Wright et al. (1987) that the Hudson Bay–Hudson Strait system generates a Helmholtz-like resonance response as it adjusts

to variations in atmospheric pressure. Our "wind-only" experiments show that the wind forcing within the Hudson Bay-Hudson Strait system is also important at this frequency band and must be included in explaining the Bay/Strait system influence.

The cross-shelf behavior of the model shows a decreasing coherence with observation toward the shelf break, consistent with the work of de Young et al. (1992). The propagation and scattering of coastal trapped waves (CTWs) are relevant to explain the along-shelf behavior of the models. Discrepancies between model results and observation on the Shelf indicate that the topography used in our model experiments (same as that used by Bryan and Holland (1989) in their eddy-resolving general circulation model) is not correctly representing the rugged topography of the Labrador Shelf.

Bibliography

Akima, H., 1978: A method of bivariate interpolation and smooth surface fitting for irregularly distributed data points. *ACM Transactions on Mathematical Software*, **4**(2), 148-159.

Anderson, D. T. L., K. Bryan, A. E. Gill, and R. C. Pacanowski, 1979: The transient response of the North Atlantic: Some model studies. *Journal of Geophysical Research*, **84**, 4795-4815.

Anderson, D. T. L., and R. A. Corry, 1985: Seasonal transport variations in the Florida Straits: A model study. *Journal of Physical Oceanography*, **15**, 773-786.

Battisti, D. S., and B. M. Hickey, 1984: Application of remote wind-forced coastal trapped wave theory to the Oregon and Washington coasts. *Journal of Physical Oceanography*, **14**, 887-903.

Blaha, J. P., 1984: Fluctuations of monthly sea level as related to the intensity of the Gulf Stream from Key West to Norfolk. *Journal of Geophysical Research*, **89**, 8033-8042.

Böning, C. W., R. Döscher, and R. G. Budich, 1991: Seasonal transport variation in the western subtropical North Atlantic: Experiments with an eddy-resolving model. *Journal of Physical Oceanography*, **21**, 1271-1289.

Bryan, F. O., and W. R. Holland, 1989: A high resolution simulation of the wind- and thermohaline driven circulation in the North Atlantic Ocean. *Parameterization of Small-Scale Processes. Proc. 'Aha Huliko'a, Hawaiian Winter Workshop*, P. Müller, and D. Henderson, Eds., University of Hawaii at Manoa, 99-115.

Bryan, K., 1969: A numerical method for the study of the circulation of the world ocean. *Journal of Computational Physics*, **4**, 347-376.

Church, J. A., H. J. Freeland, and R. L. Smith, 1986: Coastal-trapped waves on the east Australian continental shelf. *Journal of Physical Oceanography*, **16**, 1929-1943.

Clarke, A. J., 1977: Observational and numerical evidence for wind-forced coastal trapped long waves. *Journal of Physical Oceanography*, **7**, 231-247.

Cox, M. D., 1984: a primitive equation, three-dimensional model of the ocean. *GFDL Ocean Group Technical Report*, **No.1**, GFDL/Princeton University, USA.

Csanady, G. T., 1982: *Circulation in the Coastal Ocean.* D. Reidel Publishing Company, 279 pp.

de Young, B., R. J. Greatbatch, A. Goulding and K. Venguswamy, 1992: Bottom pressure variability on the Labrador Shelf: Model-data comparisons. *Journal of Geophysical Research*, **97**, 11323-11331.

de Young, B., R. J. Greatbatch, and H. T. Wareham, 1994: Departures from the inverse barometer in a global barotropic ocean model driven by atmospheric pressure forcing. *Journal of Geophysical Research*, submitted.

Fanning, A. F., R. J. Greatbatch, A. M. da Silva, and S. Levitus, 1991: Model-calculated seasonal transport variations through the Florida Straits: A comparison using different wind stress climatologies. *Journal of Physical Oceanography*, **24**, 30-45.

Garrett, C., F. Majaess, and B. Toulany, 1985: Sea-level response at Nain, Labrador, to atmospheric pressure and wind. *Atmosphere-Ocean*, **23**, 95-117.

Gill, A. E., 1982: *Atmosphere-Ocean Dynamics*. Academic Press, 662 pp.

Gill, A. E., and P. P. Niiler, 1973: The theory of the seasonal variability in the ocean. *Deep-Sea Research*, **20**, 141-177.

Greatbatch, R. J., and A. Goulding, 1989: Seasonal variations in a linear barotropic model of the North Atlantic driven by the Hellerman and Rosenstein wind stress field. *Journal of Physical Oceanography*, **19**, 572-595.

Greatbatch, R. J., B. de Young, A. Goulding, and J. Craig, 1990: On the influence of local and North Atlantic wind forcing on the seasonal variation of sea level on the Newfoundland and Labrador Shelf. *Journal of Geophysical Research*, **95**, 5279-5289.

Greatbatch, R. J., and J. Li, 1990: Barotropic variability in the presence of an ocean gyre. *Journal of Marine Research*, **48**, 37-53.

Heaps, N. S., 1971: On the numerical solution of the three-dimensional hydrodynamical equations for tides and storm surges. *Mémoires Société Royale des Sciences de Liège*, **I**, 143-180.

Hellerman, S., and M. Rosenstein, 1983: Normal monthly wind stress over the world ocean with error estimates. *Journal of Physical Oceanography*, **13**, 1093-1104.

Huthnance, J. M., 1992: Extensive slope currents and the ocean-shelf boundary. *Progress in Oceanography*, **29**, 161-196.

Ikeda, M., 1987: Modeling interpretation of mesoscale meanders of the ice edge off the Labrador coast observed in NOAA satellite imagery. *Journal of Physical Oceanography*,**17**, 1468-1483.

Killworth, P. D., D. Stainforth, D. J. Webb, and S. M. Paterson, 1991: The development of a free-surface Bryan-Cox-Semtner ocean model. *Journal of Physical Oceanography*, **21**, 1333-1348.

Large, W. G., and S. Pond, 1981: Open ocean momentum flux measurements in moderate strong winds. *Journal of Physical Oceanography*, **11**, 324-336.

Larsen, J. C., 1992: Transport and heat flux of the Florida Current at $27^{\circ}N$ derived from cross-stream voltages and profiling data: Theory and observations. *Philosophical Transactions of the Royal Society of London, A*, **338**, 169-236.

LeBlond, P. H., 1982: Satellite observations of Labrador Current undulations. *Atmosphere -Ocean*, **20**, 129-142.

Lee, T. N., and E. Williams, 1988: Wind-forced transport fluctuations of the Florida Current. *Journal of Physical Oceanography*, **18**, 937-946.

Maul, G. A., D. A. Mayer, and M. Bushnell, 1990: Statistical relationships between local sea level and weather with Florida-Bahamas cable and Pegasus measurements of Florida Current volume transport. *Journal of Geophysical Research*, **95**, 3287-3296.

Mesinger, F., and A. Arakawa, 1976: *Numerical Methods Used in Atmospheric Models, Vol.I.* WMO-ICSU Joint Organizing Committee, GARP Publications Series No.17, 64 pp.

Middleton, J. F., and D. G. Wright, 1989: Coastally trapped waves on the Labrador Shelf. *Canadian Technical Report of Hydrography and Ocean Sciences*, **116**, vi+76 pp.

Middleton, J. F., and D. G. Wright, 1991: Coastal-trapped waves on the Labrador Shelf. *Journal of Geophysical Research*, **96**, 2599-2617.

Molinari, R. L., F. Chew, W. D. Wilson, M. Bushnell, D. Mayer, K. Leaman, F. Schott, T. Lee, R. Zantopp, J. C. Larsen, and T. Sanford, 1985: Subtropical Atlantic climate studies: Introduction. *Science*, **227**, 292-294.

Niiler, P. P., and W. S. Richardson, 1973: Seasonal variability of the Florida Current. *Journal of Marine Research*, **31**, 144-167.

Pares-Sierra, A., and J. O'Brien, 1989: The seasonal and interannual variability of the California Current system. *Journal of Geophysical Research*, **94**, 3159-3180.

Ponte, R. M., D. A. Salsten, and R. D. Rosen, 1991: Sea level response to pressure forcing in a barotropic numerical model. *Journal of Physical Oceanography*, **21**, 1043-1057.

Ponte, R. M., 1993: Variability in a homogeneous global ocean forced by barometric pressure. *Dynamics of Atmospheres and Oceans*, **18**, 209-234.

Schott, F. A., T. N. Lee, and R. Zantopp, 1988: Variability of structure and transport of the Florida Current in the period range of days to seasonal. *Journal of Physical Oceanography*, **18**, 1209-1230.

Thompson, K. R., 1986: North Atlantic sea-level and circulation. *Geophysical Journal of Royal Astronomical Society*, **87**, 15-32.

Thompson, J. R., N. Lazier, and B. Taylor, 1986: Wind-forced changes in Labrador Current transport. *Journal of Geophysical Research*, **91**, 14261-14268.

Wang, D. P., and C. N. K. Mooers, 1976: Coastal-trapped waves in a continuously stratified ocean. *Journal of Physical Oceanography*, **6**, 853-863.

Webster, I., and S. Narayanan, 1988: Low-frequency current variability on the Labrador Shelf. *Journal of Geophysical Research*, **93**, 8163-8173.

Wunsch, J., S. G. H. Philander, and R. C. Pacanowski, 1980: The oceanic response to large-scale atmospheric disturbances. *Journal of Physical Oceanography*, **10**, 411-429.

Wright, D. G., D. A. Greenberg, and F. G. Majaess, 1987: The influence of bays on adjusted sea level over adjacent shelves with application to the Labrador Shelf. *Journal of Geophysical Research*, **92**, 14610-14620.

Wright, D. G., J. R. N. Lazier, and W. Armstrong, 1988: Moored current and pressure data from the Labrador/Newfoundland Shelf, June 1985-July 1987. *Canadian Technical Report of Hydrography and Ocean Sciences*, **62**, x+258 pp.

Wright, D. G., D. A. Greenberg, and J. F. Middleton, 1991: statistical estimates and dynamical interpretations of bottom pressure variations over the Labrador /Newfoundland Shelf. *Canadian Technical Report of Hydrography and Ocean Sciences*, **131**, v+60 pp.